Conversion of Chromium Ore Processing Residue to Chrome Steel

Final Report

Submitted by

Dr. Jay N. Meegoda, P.E.
Dr. Zhengbo Hu and Dr. Wiwat Kamolpornwijit
Dept. of Civil & Environmental Engineering
New Jersey Institute of Technology
Newark, NJ 07102

For the New Jersey Department of Environmental Protection

NJDEP Project Manager: Mr. Robert T. Mueller

December 2007

New Jersey Institute of Technology

TABLE OF CONTENTS

Conversion of Chromium Ore Processing Residue to Chrome Steel

Introduction

Chromium played an important role in the industrial development of New Jersey from 1905 to 1971. During that period, chromate (Cr^{6+}) was produced from chromite ore at three facilities in Hudson County, NJ. During the chromate extraction process, varying amounts of lime and soda ash were added and roasted with pulverized chromite ore to a temperature between 1100°C and 1150°C under an oxidizing environment. Trivalent chromium in chromite ore was oxidized to hexavalent chromium. The highly soluble hexavalent chromium was then removed from the COPR (left over Chromium Ore Processing Residue) leaving un-oxidized trivalent chromium and slow-dissolving hexavalent chromium compounds [Burke et al., 1991]. In the absence of information on the toxicity of hexavalent chromium, COPR was subsequently used for the back-filling of demolition sites, preparation for building foundations, construction of tank berms, roadway construction, the filling of wetlands, and other construction and development related purposes.

The US Environmental Protection Agency (EPA) has classified hexavalent chromium as a Group A Human Carcinogen. Some forms of hexavalent chromium are water soluble in the full pH range, while trivalent chromium tends to be absorbed onto COPR sample surface or precipitate as chromium hydroxide in slightly acidic and alkaline environment. The highly soluble hexavalent chromium in COPR poses a large threat to environment and public health. Currently COPR contamination has been found in many sites on interior and exterior walls, building floors, surfaces of driveways and parking lots, and on the surface and subsurface of unpaved areas throughout Hudson County. The New Jersey Department of Environmental Protection (NJDEP) has identified over 150 sites in Hudson County where COPR is still present. These sites have concentrations of chromium ranging from a few parts per million to about 5 percent by weight. Current NJDEP estimates that there are more than ten million tons of environmentally weathered and mixed COPR, commonly referred to as chromium contaminated soils, in Hudson County, NJ.

Several technologies were developed for treating of chromium contaminated media including, but not limited to, stabilization, vitrification, electro-kinetic treatments, separation, soil washing, and bioremediation. The treatment technology may be specifically effective towards certain

kinds of chromium contaminated soils depending on chromium oxidation states, phases, and media compositions.

This report summarizes the characteristics of chromite ore processing residue (COPR) in terms of their chemical compositions and phases and results from the melting study to convert to iron with chromium or steel.

The COPR from three hazardous waste sites in Jersey City, New Jersey, were analyzed using non-destructive instruments including scanning electron microscopes (SEM), x-ray diffraction spectrometers (XRD), and x-ray fluorescence spectrometers (XRF).

The physical and chemical characterization of environmentally weathered COPR will fundamentally benefit both remediation and beneficial use of chromium contaminated soils. This knowledge will enable rapid development of efficient technology for treatment of environmentally weathered COPR, i. e., smelting reduction of iron oxide to produce iron with chromium.

A literature search of separation and concentration of chromium and iron from soil was performed. The literature search revealed that melting would itself separate the iron and chromium from COPR leaving the remainder as slag.

The reduction tests using milligram specimens were performed in the Thermo-Gravimetric Analyzer (TGA) where the samples were placed in graphite crucibles and flushed with nitrogen to create an oxygen-free environment. TGA was used as a furnace that supplies high heat under a controlled environment and to study reductions under different conditions and the comparisons in reduction behaviors of different oxides. The use of solid carbon as a reducing agent has both advantages and disadvantages. The solid carbon uncontrollably reacts with iron oxide in COPR at high temperature.

The TGA test data and phase separation data were refined using scaled-up test specimens in high temperature furnace. Over ten samples of blended COPR were melted to make chromium steel. After melting, the composition of chrome iron and the remaining waste were analyzed using XRF to determine chromium concentration in iron and in the waste. Steel and waste

samples were tested using ESEM with EDX to obtain the distribution of chromium in waste and also in the chrome iron.

Literature Search

This literature survey mostly covers studies on chromite ore reduction during the past 20 years. The kinetics of reduction of chromite ore plays an important role in controlling the productivity of the processes and quality of Ferro-chromium. A considerable amount of research has been carried out on the carbothermic reduction of chromite ore to elucidate the kinetics and mechanism of the reduction process. The influence of different parameters such as time, temperature, chemical composition, addition of carbon, particle size of ore and carbon etc. on the rate of reduction has been studied. The feasibility and the mechanics of the reduction of iron and chromium oxide are determined using Ellingham Diagram.

Ellingham Diagram and Reduction of Iron Oxide

The standard free energy change for any reaction, for example $2Fe + O_2 \rightarrow 2FeO$, can be expressed in terms of the standard enthalpy and entropy changes:

$$\Delta G^\circ = \Delta H^\circ - T\Delta S^\circ \qquad (1)$$

The standard free energy change of reaction, ΔG^o, is expected to be linear with a slope equal to $-\Delta S^o$ and an intercept at T = 0°K equal to ΔH^o, provided there is little change on ΔH^o and ΔS^o.

In the Ellingham Diagram (**Figure 1**), the change in slope of the free energy lines at certain temperature is due to the latent heat from melting, boiling, transition, or sublimation. The negative slope reflects the positive ΔS°; $d(\Delta G^\circ) / dT = -\Delta S^\circ$, due to the increasing volume after the reaction, for example $2C + O_2 = 2CO$.

When carbon is used as reducing agent for metal oxide reduction, the reaction will favor a higher temperature because, for the reaction $C + FeO \rightarrow Fe + CO$

$$\Delta G_{C + FeO \rightarrow Fe + CO} = \Delta G_{2C + O2 = 2CO} - \Delta G_{2Fe + O2 \rightarrow 2FeO} \qquad (2)$$

The Ellingham Diagram can be used to determine the relative ease of reducing a given metallic oxide to metal. The order of oxides in term of their stability at 1400°C is $CaO > Al_2O_3 > MgO > SiO_2 > MnO > Cr_2O_3 > FeO > Fe_3O_4 > Fe_2O_3$.

The reducing environment is essential for metal oxide reduction to metal. As shown in equation 3, the oxygen partial pressure should be low enough for preventing the metal to oxidize back to metal oxide.

$$\Delta G^{o}_{M+O_2->MO} = -RT\ln\left(\frac{1}{p_{O_2}^{1/2}}\right) \quad (3)$$

When carbon or CO is used as reducing agent, for the reduction of iron oxide to proceed, the ratio of CO_2/CO has to be adjusted to keep the low oxygen partial pressure according to the C-O_2-CO-CO_2 equilibrium system (**Table 1**).

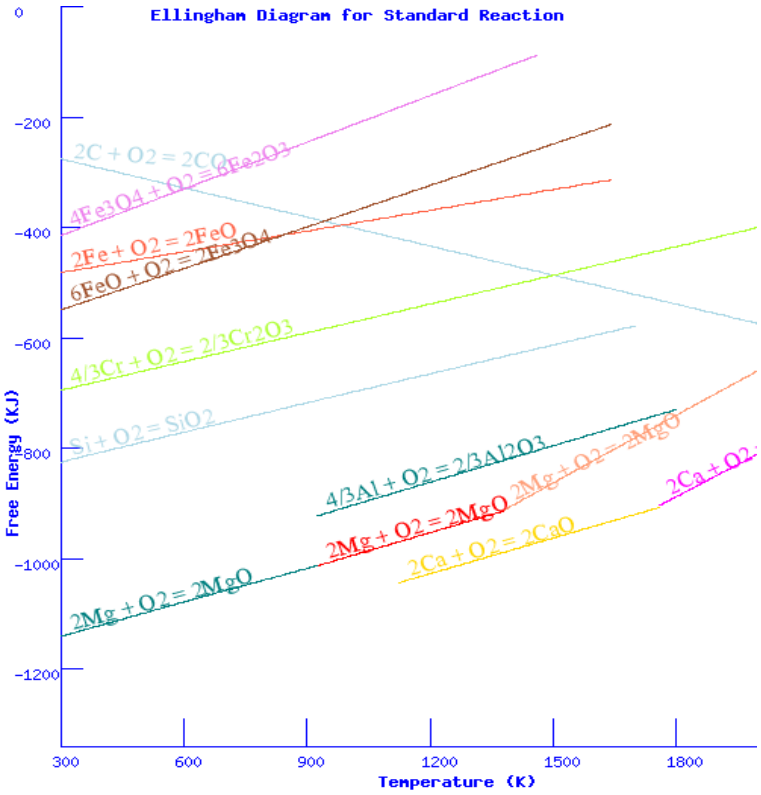

Figure 1. Ellingham Diagram of Metal Oxides

Ellingham diagram and **Table 1** also show the thermodynamic feasibility for iron and chromium reduction to metal at temperature up to 1500°C with carbon as the reductant. More details will be discussed later on the intermediate carbide compound and step-by-step reaction. Since the melting point of Fe-Cr alloy will be lower than the melting point of Fe or Cr (1530-1475°C based on the Cr content), it is possible to separate metal from slag with proper chemical compositions at temperature less than 1600°C.

Table 1. Comparison of the melting point and metal formation by reduction

	MP of Metal (^oC)	**BP of Metal** (^oC)	**T1** (^oC)	**P_{O2}**	**CO/CO_2**
Fe	1530 1350 for FeO	2861	730	10^{-9}	9
Cr	1907	2671	1230	10^{-12}	$7*10^2$
Si	1414 1710 for SiO2	2900	1620	10^{-17}	$5*10^4$
Mg	650	1090	1850	10^{-21}	$5*10^6$
Al	659	2519	2000	10^{-21}	$7*10^6$
Ca	842	1484	>2000	10^{-25}	$8*10^8$
C	3600	-	/	/	/

- **MP** = Melting point**; BP** = boiling point
- **T1** is the temperature at which C can reduce metal oxide to metal and CO. ($\Delta G_{MO+C \rightarrow M+CO}=0$)
- **P_{O2}** is the partial pressure of oxygen that is in equilibrium with metal and metal oxide at 1600 ^0C.
- **CO/CO_2** is the ratio CO to CO_2 that will be able to reduce the oxide to metal at 1600 ^oC.
- **P_{O2} and CO/CO_2** value can be easily obtained from more complete Ellingham Diagram

Effect of Reductant (C/CO)

When carbon is heated with metal oxide (for example Fe_2O_3) at high temperatures under a reduced environment, the reduction of Fe_2O_3 occurs either by direct reduction with carbon or indirect reduction with gaseous CO. The direct reaction is given by $Fe_2O_{3(molten)} + 3C_{(solid)} = 2Fe_{(metal)} + 3CO_{(gas)}$ and the indirect is given by $Fe_2O_{3(molten)} + 3CO_{(gas)} = 2Fe_{(metal)} + 3CO_{2(gas)}$. In an indirect reduction, the gasification of carbon through the endothermic Boudouard reaction ($C+CO_2 \rightarrow 2CO$) plays a very important role on the reduction rate.

The direct reduction occurs at the interface between iron oxide and solid carbon. Nonetheless, the contact between them is not continuous due to the product formation. This can cause a marked decrease in the reduction rate in relation to the progress of reaction. Bogdandy and Engell (1971) reviewed literature and concluded that the direct reduction had no importance in the industrial reduction process. It rather took place as part of a chain reaction. Literatures (Srinivasan and Lahiri, 1977; Szendrei and Van Berge, 1988) suggested that the indirect reduction governed and the reduction rate was limited by the carbon gasification.

However, there are some researchers who stressed the significance of the direct reduction. Sugata et al. (1974) studied the smelting reduction of FeO in molten slag by rotating a solid carbon disk. The reduction of iron oxide at the interface of molten slag and solid carbon disk resulted in the CO gas formation. The CO bubbles acted as a barrier for the direct contact between iron oxide and carbon. They found that *the reduction rate increased as they evacuated CO*, allowing the direct contact between iron oxide and solid carbon.

Bafghi (1993) found that the rate of reduction of FeO increased with the evacuation of CO (produced as a product of FeO/Fe_2O_3 reduction). The occurrence of CO enhanced the agitation and thus promoted the reduction at low concentration of FeO (2%), but acted as a barrier between the molten iron oxide and solid carbon at higher FeO concentrations.

Weber (1993) has also demonstrated that the chromite ore cannot be reduced by CO gas alone, in the absence of carbon. The ore can be reduced by carbon, but the reaction may proceed through two steps: $FeCrO_4 + 4C \rightarrow Fe + 2Cr + 4\ CO_2$ and $C + CO_2 \rightarrow 2CO$.

<u>Carbon: the reductant amount / size / type</u>

Ding (1997) used graphite bought from Aldrich Chemical. The weight ratio of graphite to chromite (40% Cr_2O_3, 24% Fe_2O_3) in the composite pellets was 0.21, which was about 10% in excess of the stoichiometric requirement for the reduction of Cr and Fe to the M_7C_3-type carbides.

Chakraborty (2002) found an increase in the reduction with addition of more carbon because reduction thermodynamically favors the generation of iron and chromium carbides, which require more carbon. However, the initial permeability of mixture (ore+carbon) decreases with the increasing addition of fine carbon, which hinders the outward transport of the gaseous reduction products. This may be one of the reasons for the reduction rate decreasing with too much carbon addition (in the paper, > 80% carbon). At higher proportions of coke, it is also possible that the finer carbon powder becomes agglomerated and thus reduces the reduction rate.

Chakraborty (2005) also investigated the reduction of chromite ores using different reducing reagents (petroleum coke, devolatilized coke - DVC and graphite) in the temperature range

1173 to 1573^{o}K. Rate of reduction was highest when raw petroleum coke was used due to the high surface area, and lowest when graphite was used.

Effect of Chemical Composition

The COPR samples obtained from nine contaminated sites in New Jersey on average had more than 29% iron and 7% chromium (Meegoda 1999). Due to the chromium extraction process, a large concentration of sodium and calcium, and small quantities of silica, aluminum and magnesium are also present in COPR samples. XRD characterization showed that metal oxides existed in the COPR in the form of spinel ($AO.B_2O_3$) or other mineral compounds. Generally, the substances which are considered basic oxides are those which are compounds of the elements forming basic compounds in ordinary chemical reactions in water solution, i.e. CaO, MgO, and Na_2O. The SiO_2 is an example of acidic flux. There are compounds of elements, for example alumina, that act both as an acid and base depending on the slag composition.

Both metal oxide reduction and metal separation are important in the iron and steelmaking process. The chemical composition of COPR determines the material properties such as basicity and viscosity. It will influence the kinetics rate for the metal reduction, and also play an important role in the separation of metal from slag. Most of the impurities, such as oxides, have very high melting temperatures; i.e. 1600°C for SiO_2. The separation of impurities requires the formation of intermediate compounds having lower melting point, sometimes by addition of compounds to change the chemical composition of the mixture.

Effect of Silica and Lime Addition on Metal Oxide Reduction

The effect of silica (acidic) and lime (basic) on the carbothermic reduction process had been studied extensively. Mroz (1994) studied the effect of CaO/SiO_2 basicity, viscosity, and temperature on the reduction rate. The rate of reaction was found to be first order with time and second order with basicity (for basicity less than 1.54). The increasing basicity increased FeO activity, and low viscosity increased the reaction rate and transportation. The maximum rate reaction occurred at basicity of 1.05 at which the lowest viscosity was obtained. The basicity of intermediate compound, $CaO.SiO_2$, is 1.0 which is similar to the above basicity value of 1.05 for maximum rate reaction.

Murti (1982) investigated the effect of lime addition on the reduction of chromites by graphite at 1200-1300°C. They found that the enhancement of the reduction is due to lime going into the spinel lattice and releasing the FeO, thereby increasing the chromite reducibility. The reduction rate and extent were found to increase all the way with increasing lime addition up to 15% with respect to chromite.

Ding (1997a and b) investigated in detail the catalytic effect of lime and silica in chromite reduction The results suggested that lime rather than SiO_2 should be used in the pre-reduction stage, however the addition of SiO_2 in the smelting stage would be an advantage.

The catalytic effect of lime on the reduction of carbon-chromite composite pellets was investigated at 1270-1433^{0}C using argon (Ding 1997). It was possible for lime to go into the spinel lattice and release FeO, as well as possibly to catalyze the chromite reduction by enhancing the nucleation and/or interfacial reaction in the early stage (the apparent activation energy ranging from 139 to161 kJ/mol depending on the amount of lime addition), and facilitate the solid-diffusion process in the later stage. The initial rate of reduction increased with increasing reduction temperatures and lime addition. The apparent activation energy (E_i) decreases with increasing additions of lime (142 for 0.4% CaO, while 84 kJ/mol for 13% CaO), indicating that lime has a catalytic effect on the chromite reduction. Lime may improve nucleation and/or chemical reaction in the first stage, but does not change the rate-limiting step.

The reduction of carbon-chromite composite pellets with a silica flux was investigated at 1240-1410^{o}C under an Argon-CO atmosphere. This was carried out in two stages, with the first stage covering a reduction level of 30-40% and not affected by the silica addition. This stage was most likely controlled by nucleation and/or chemical reaction with apparent activation energy of 172kJ/mol. However, during the second stage the effect of silica was noted at a temperature equal to or greater than 1380°C. Silica influenced the reduction kinetics in the second stage through the formation of a liquid slag. The effect of the amount of silica addition on the reduction was due to the competing effects of an enhanced chromite reduction owing to the formation of a liquid phase on one hand, and the liquid phase blocking the outward transport of gaseous reduction products on the other. In summary, lime (CaO) may improve nucleation and/or chemical reaction in the first stage, due to the lime entering into the spinel lattice and releasing the FeO, thereby increasing the chromite reducibility. Addition of lime does not change the rate-limiting step.

The characterization of COPR in various New Jersey sites showed large excess of CaO (15-32%) due to the chromate extraction process (Meegoda 1999). So no additional lime is needed for the metal (Fe/Cr) reduction process at a high temperature (~1500^{o}C). The relative large amount of Al_2O_3 (15-20%) is comparable to the chromite ores which were used by other research groups. There is no report on the catalytic effect of Al_2O_3 on reduction rate of Fe/Cr, so alumina mainly plays an important role in the formation of liquid slag at lower temperatures. Due to the high basicity of the COPR in our research, sand (SiO_2) addition may be necessary for the liquid slag formation in the late stage of reduction.

Effect of Chemical Composition on Metal Separation

Slag is an important part for metal separation of and steel quality. In steelmaking industry, the slag removes unwanted oxides, sulphides, nitrides and phosphides, and also provides a cover to protect refined steel from reoxidation and nitrogen and hydrogen pickup. Since the ultimate goal of this project is to reduce and recover the metal (almost all Fe / Cr) and separate from the slag, the slag compositions must be closely controlled to achieve a low slag liquidus temperature.

The factors governing the metal separation include but are not limited to the melting temperature and slag viscosity, which depend on slag compositions. The behavior of slag or oxide system can be partly described through phase diagrams which are great tools in understanding the behavior and property of slag at equilibrium at different temperatures.

Lekatout (1995) reported the pre-reduction and metal separation of chromite concentrate (49% Cr_2O_3, 11% Fe_2O_3, 4% FeO, 9% Al_2O_3, 18% MgO, 7% SiO_2, 0.2 % CaO). The pre-reduction was performed on chromite briquettes with ~25% graphite at 1400^{0}C for 2 hours, with 75% reduction percentage. The maximum metallization of iron and chromium was 91% and 67%, respectively. The main reduction products characterized by XRD were: (1) metallic products, in order of succession of formation, Fe-C alloy, $(Cr, Fe)_7C_3$, and $(Cr, Fe)_{23}C_6$; (2) non-metallic products, forsterite, Spinel $MgAl_2O_4$, chromite spinel. Excess graphite (1.6 $\times$ stoichiometric) will not help increase reduction percentage.

The metal separation study performed by Lekatout (1995) turned out to be very successful for the pre-reduced chromite. In their research, melting of the 72.5% pre-reduced chromite

concentrate with 25% silica, at 1550^0C for 1.5 h, led to 97.5% chromium recovery and 100% iron recovery. The expected composition of the slag after the addition of 25% of SiO_2 is 15%Al_2O_3, 31% MgO and 54% SiO2, belonging to a forsterite with a liquidus temperature of 1500^0C, see the phase diagram of the system Al_2O_3-MgO-SiO_2. Further characterization of the alloy indicated the silicon content is low (2.6% by weight) and the carbon content (7.0%) lies within ASTM specifications.

In our research the slag components of interest are CaO, MgO, SiO_2, and Al_2O_3, **Table 2.**

Table 2. Concentration of Major Metal Oxides in COPR Samples (% wt) (Meegoda 1999)

Site	MgO	Al_2O_3	SiO_2	CaO	Cr_2O_3	Fe_2O_3
LSP	12.7	14.6	2.6	14.9	9.4	43.5
CD	7.8	17.6	12.9	31.2	5.9	19.5

*LSP = Liberty State Park, CD = Colony Diner

The COPR is rich with CaO and/or MgO, the basic oxides. So the addition of sand (SiO_2), an acid oxide to COPR should bring the melting temperature down and ease the agglomeration of the metallic iron.

Figures 2a-2d shows the liquidus isotherms of a quaternary system, CaO-MgO-SiO_2-Al_2O_3, represented by several ternary systems, each with a constant concentration of Al_2O_3. The shaded areas are bounded by the liquidus isotherm at 1500°C. The formation of intermediate compounds by mixed oxides helps lower the melting temperature. There are large composition ranges of COPR within shaded areas that could melt and possibly allow the metal separation. Due to large excess of CaO (and/or MgO) for COPR in New Jersey sites, additional SiO_2 (sand) will be needed to reach the right chemical composition within the shaded area.

It is noteworthy to realize that upon the melting of the intermediate compound, the other oxides can dissolve into the liquid mass and change the viscosity or fluidity. Lower viscosity of liquid slag helps metal separation. Lower melting points of intermediate compounds and addition of CaF_2 help lower the viscosity of melting mixture.

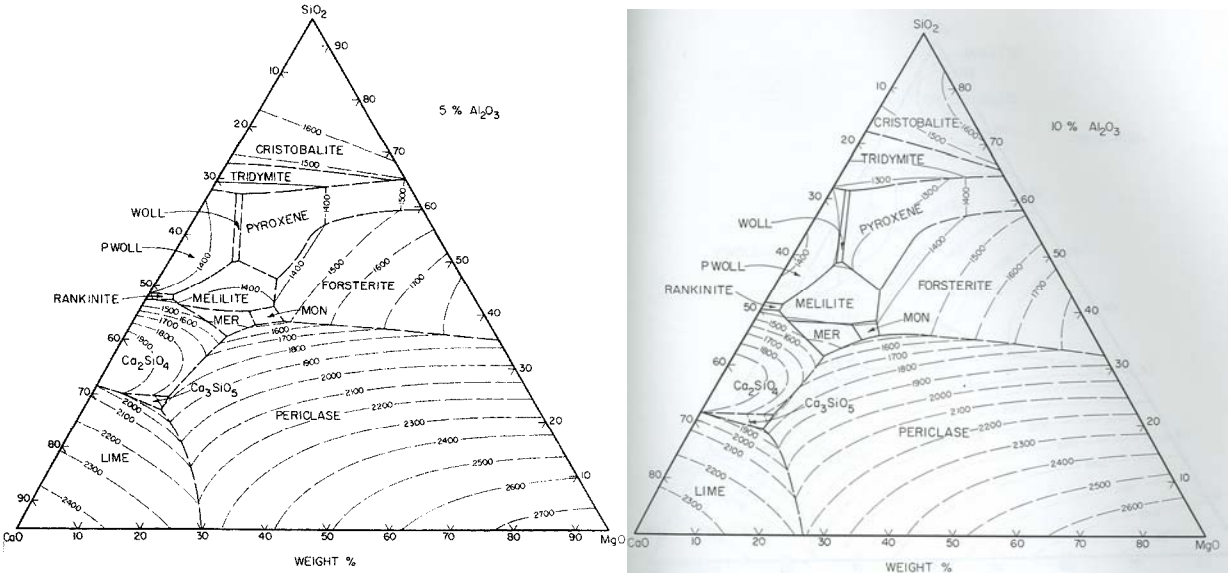

(a) 5% Al_2O_3 (b) 10% Al_2O_3

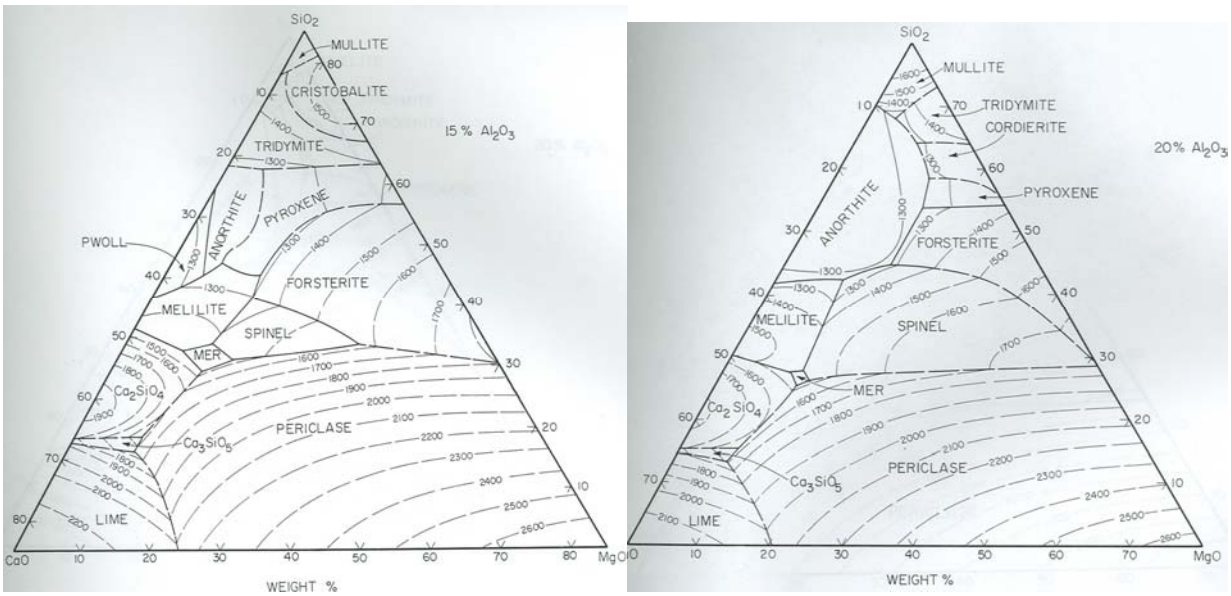

(c) 15% Al_2O_3 (d) 20% Al_2O_3

Figure 2 Liquidus Temperatures of a CaO-SiO_2-MgO-Al_2O_3 System in a Constant Concentration Plane at 5% - 20% Al_2O_3 (Muan and Osborn, 1985)

Fe/Cr and Carbide Intermediates

The reduction of chromite by carbon can be represented, in a simple form, by $FeCrO_4 + 4C \rightarrow Fe + 2Cr + 4\ CO$. Usually carbides are formed by the reduction of the oxides and this can be represented by $21FeCrO_4 + 100C \rightarrow 7Fe_3C + 3Cr_7C_3 + 84\ CO$. In all cases iron was preferentially reduced in the early stages of reduction. Reduction of iron led to the formation of

either a liquid metal or a carbide. Formation of both these phases enhanced the reduction of chromium. Presence of an iron alloy helped to reduce the activity of chromium through the formation of Fe-Cr-C alloy. Formation of mixed carbides of iron and chromium also favored the reduction of chromium thermodynamically. The liquid alloy and the carbides acted as reducing agents and carriers of carbon, thereby enhancing the rate of reduction (Chakraborty 2004).

Table 3. Standard Free energies and equilibrium Temperatures of reactions during carbothermic reduction of chromite. (*For a more complete table*, *see [Lekatou 1995])*

		T (K) at P_{CO} (atm)			
Equation	**ΔG^o_T (KJ)**	**1**	**0.1**	**0.01**	**0.001**
$3\ Fe_2O_3 + C = 2\ Fe_3O_4 + CO$	137 – 0.23 T	603	557	517	482
$Fe_2O_3 + C = 2\ FeO + CO$	180 – 0.22 T	824	757	701	652
$Fe_3O_4 + C = 3\ FeO + CO$	201 – 0.21 T	942	865	799	742
$FeO + C = Fe + CO$	153 – 0.15 T	1001	890	801	728
$Fe_3O_4 + 5\ C = Fe_3C + 4\ CO$	671 – 0.68 T	983	884	803	735
$3\ FeO + 4\ C = Fe_3C + 3\ CO$	470 – 0.47 T	1001	892	804	732
$FeO + Fe_3C = 4\ Fe + CO$	143 – 0.14 T	1000	882	789	713
$3\ Cr_2O_3 + 13\ C = 2\ Cr_3C_2 + 9\ CO$	2306 – 1.5 T	1557	1395	1263	1154
$7\ Cr_2O_3 + 27\ C = 2\ Cr_7C_3 + 21\ CO$	5426 – 3.5 T	1571	1407	1274	1164
$23\ Cr_2O_3 + 81\ C = 2\ Cr_{23}C_6 + 69\ CO$	18153 – 11.3 T	1613	1443	1306	1193
$Cr_2O_3 + 3\ C = 2\ Cr + 3CO$	825 – 0.49 T	1698	1518	1373	1253
$3\ Cr_2O_3 + 13\ Fe_3C = 2Cr_3C_2+39Fe+9\ CO$	2172 – 1.3 T	1610	1427	1282	1164
$Cr_2O_3 + 3\ Fe_3C = 2\ Cr + 9\ Fe + 3\ CO$	794 – 0.46 T	1743	1548	1392	1265
$3\ Cr_2O_3 + 3\ Cr_7C_3 = Cr_{23}C_6 + 3\ CO$	937 – 0.45 T	2095	1857	1667	1513
$23\ FeCr_2O_4 + 104\ C = 23\ Fe + 2\ Cr_{23}C_6 + 92\ CO$	21677- 15 T	1467	1311	1185	1081
$FeCr_2O_4 + 4\ C = Fe + 2\ Cr + 4\ CO$	978 – 0.64 T	1531	1367	1235	1126
$FeCr_2O_4 + 4\ Fe_3C = 13\ Fe + 2\ Cr + 4\ CO$	937 – 0.6 T	1566	1388	1246	1131

The standard free energies of the possible reactions during chromite reduction as a function of temperature and the equilibrium temperatures at various CO partial pressures have been calculated from the available thermodynamic data (**Table 3**). Ideal behavior was assumed, since little is known about the activities of the oxides in the spinel structure. The possible iron/chromium carbides listed in the equation had been identified by X-ray diffraction patterns

obtained from various stages of reduction (Lekatou 1995). Under reduced CO partial pressures, the reduction reactions occur at lower temperatures.

The Percentage Reduction %R is usually calculated as %R = [W(t)-W(v)] / W * 100, where W(t) = observed weight loss of sample at time t, W(v) = weight loss due to volatile material of reductant and chromite and W = theoretical weight loss for complete reduction of iron oxide, chromium oxide to Fe^{o} and Cr^{0} respectively.

The percentages of iron and chromium in the metallic and non-metallic products can be determined by wet chemical methods and atomic absorption (AA) spectroscopy (Perkin-Elmer spectrophotometer). The reduced samples can be characterized by Philips 1710 XRD diffractrometer (in the form of powder) and scanning electron microscopy (SEM).

To determine the kinetics of reduction of chromite, the percentage metallization at various time intervals were substituted into equations defining different kinetics of reduction.

(1) for diffusion-controlled reaction: $1-2/3x-(1-x)^{2/3} = kt$
Zhuravlev-Lesokhin-Tempel'man equation $[1/(1-x)^{1/3} - 1]^2 = kt$
(model for solid-diffusion control – Ding 1997)

(2) for nucleation-controlled reaction: $-\ln(1-x) - kt$

(3) For chemical-reaction-controlled reaction: $1-(1-x)^{1/3} = kt$

(4) For Jander diffusional model: $[1-(1-x)^{1/3}]^2 = kt$

Where, x=fraction of reduction, k = rate constant, t = time.

The activation energy for the process was evaluated using the Arrhenius equations:

$$k = A * \exp(-E/RT)$$

Where k is the rate constant, E is the activation energy, T is the temperature, and A is the pre-exponential factor.

Table 4 shows some kinetics results from a few research groups on carbothermic reduction of chromite ore. The composition of the ore, temperature ranged studied, and the kinetic mechanism and activation energy were listed for comparison.

Table 4. Reduction Kinetics studied by various investigators

Composition of Ore							Temp. (°C)	Kinetic & mechanism	E_a (kJ/mol)	References
Cr_2O_3	FeO	Fe_2O_3	Al_2O_3	SiO_2	CaO	MgO				
40	-	24	15	6	0.4	15	1000-1500	Early: - nucleation Later: - Diffusion	114 221	Ding, 1997
50	3.5	11	9.2	6.6	0.2	18	1100-1470	Diffusion	---	Lekaton, 1995
46	15	11	15	1.2	-	11	1100-1500	Diffusion	190	Barcza, 1971
48	23	-	10	4	-	11	1000-1400	ZLT (diffusion)	194	Doung, 2000
50	Fe_{lot}=12		16	3.2	0.4	15	1200-1500	Diffusion	247	Verzalis /Lekatou 1993
41	21	11	18	-	-	10	NA	Ionic diffusion	-	Perry, 1988
Not available							200-1250	Early: - Jander Later: - ZLT	129 600	Van Vuuren, 1992
Not available							1300-1450	Early: - Carbon gasification Later: -Diffusion	125 238	Niyesh, 1992
Not available							1210-1300	Oxygen diffusion	-	Murti, 1985

As shown in **Table 4**, Ding (1997) concluded that the early stage of reduction up to a reduction level of 60% fit both an exponential law for nucleation control and an equation for chemical control. In the later stage after approximately 65% reduction, solid diffusion of chromium in the oxide phase is the most likely rate-controlling step with apparent activation energy of 410kJ/mol. The late stage of reduction was found to fit the ZLT equation, which is the kinetic model for solid-diffusion control. Lime is also suggested to catalyze the chromite reduction by enhancing the nucleation and/or interfacial reaction in the early stage, and facilitating the solid-diffusion process in the late stage.

Also as an example, Duong (2000) found that the early stage of reduction of Australian Chromite with coal had activation energy of 194kJ/mol. This reaction was controlled by solid-state diffusion of cations. There was a change in mechanism during the later stages of reduction caused by the formation of slag. The early stage involved mainly the reduction of iron.

During the second stage, which had activation energy of 256kJ/mol, the reduction was likely to be controlled by the dissolution of iron and chromium in the slag. Silica addition was found to enhance significantly the rate and degree of reduction at 1300 and 1400^{o}C.

Based on the literature study the following conclusions were made:

- For metal oxide reduction, lime (CaO) may improve nucleation and/or chemical reaction in the first stage (<1200^{o}C), due to the lime entering into the spinel lattice and releasing the FeO, thereby increasing the chromite reducibility. Silica (SiO_2) influenced the reduction kinetics in the second stage (at higher temperatures) through the formation of a liquid slag. The maximum rate reaction might occur at basicity of slag at around 1, at which point low viscosity could be obtained.
- For metal separation, phase diagram of a quaternary system, CaO-MgO-SiO_2-Al_2O_3, represented by several ternary systems, each with a constant concentration of Al_2O_3, is used to determine the right chemical composition for low liquidus temperature (<1500^{o}C). Sand addition will be needed.
- Variables in the experiments, such as temperature, time, chemical composition, addition of reductants (carbon), particle size of ore and carbon, etc. had been reviewed in this literature search. The reduction of COPR can be performed with stoichiometric (or a little excess) graphite under a reduced environment (N_2 or argon). The temperature for reduction will rise to 1500-1600^{o}C to ensure the full recovery of iron and chromium. The effect of CO / CO_2 gas will be investigated to optimize the reduction percentage.
- Metal separation after the reduction COPR could be achieved by the right chemical composition, and high temperatures up to 1550-1600^{o}C for 2 hours. Hence, no pre separation of COPR is needed.

Experimental Program

Sample Collection and Preparation

COPR samples, of approximately 25 gallons each, were collected from three sites in Jersey City, NJ, identified as NJDEP Site 131, NJDEP Site 115 South End, and NJDEP Site 115 North End. The samples taken from these sites were labeled Sample 1, Sample 2-S, and Sample 2-N, respectively. Sample custody documentation was performed at three stages: during the receipt of samples for testing, laboratory analysis and final evidence files. Chain-of-custody forms were signed and the project name, COPR sample weight, date and time of arrival were recorded in a bound laboratory logbook.

The samples were homogenized before measurement or testing by rigorously stirring and mixing in a mechanical mixer in High Performance Concrete Laboratory of NJIT. Subsequently 5 gallons of soil from each site were dried overnight in an oven at 80^{o}C, grinded to a fine powder using a ring grinder, and mixed homogenously. The fine powder was further manually grounded to 100-mesh ($<$80μm) for the XRD and XRF analysis. When COPR was consumed during the testing, COPR weight consumed along with the date of consumption were recorded. The particle size of the sample used in analysis and reduction was specified in the analysis section. Final evidence files, including originals of all laboratory reports and purge files, are maintained under document control.

Analytical Procedure

The characteristics of concern are chemical compositions, phases, and morphology of chromium contaminated soils, the reduced products (metal) and byproducts (slag). The homogenized COPR samples were analyzed by X-Ray Diffraction spectrometer (XRD) to obtain their phase assemblages. The chemical compositions were determined by X-ray Fluorescence (XRF) and scanning electron microscope (SEM) with Energy Dispersive X-ray (EDX) detector. The bulk chemical analysis results from XRF are compared with results from wet chemical analysis (ICP-MS) as a part of the QA/QC plan. These tests are performed in the Geo-environmental lab and Material Characterization laboratory at NJIT.

X-Ray Fluorescence spectrometer (XRF)

Wavelength dispersive XRF (Philips, PW2400), was used in this study. Being a non-destructive technique, X-ray fluorescence spectrometry has become one of the most efficient instrumental means to detect the elemental composition of inorganic, ceramic, mineral, and alloy samples. It allows the analysis of chemical composition of bulk sample regardless of the phase differences with minimal sample preparation. It is used for multi-element, qualitative, quantitative and/or semi-quantitative determinations from ppm (ca. 0.1%) to high weight percentages level elements ranging from carbon to uranium in sample matrices. It is a simultaneous spectrometer, analyzing for all specified elements in one measurement. This is possible by the mobile detector mounted on the rotating goniometer, allowing the detection of x-rays diffracted at different angles.

The elements in the sample for XRF are excited by high-energy incident x-ray beam, Rhodium tube with tungsten anode. Upon excitation, the elements emit their own characteristic x-rays, called fluorescence. The characteristic x-rays, of different energy and wavelengths, were separated by wavelength as they diffracted through the crystal of known d-spacing. The diffracted angles relate to the wavelength by Brag's Law as shown below.

$$n\lambda = 2d\sin(\theta) \quad (4)$$

where n is an integer (the full wavelength path difference between successive plane), λ is wavelength, d is d-spacing of the crystal plane perpendicular to the surface, and θ is the incident angle between the x-ray and the surface plane of the crystal.

The software package provides both full quantitative and semi-quantitative analysis. The semi-quantitative analysis of samples was performed to obtain an estimate of concentration ranges prior to preparing the standards. It is a semi-empirical calculation, which is a very useful tool for a sample of small quantity or when the standards are not available. The full quantitative analysis required a calibration against the standards. The accuracy in analyzing the sample against the calibrated standard depends on many factors including but not limited to the accuracy of the instrument, the sample preparation, the sample and standard matrix including particle size and the homogeneity of the sample, and human error.

The instrument allows two working environment; *under vacuum or helium*. The vacuum environment is better than the helium since there are less gas particles in the chamber and consequently less absorption of characteristic x-ray. The vacuum is suitable for solid sample, pressed powder, and fused glass. Helium allows the analysis of loose powder with no sample preparation. All standards and COPR samples in the report were prepared as pressed powder and analyzed under vacuum.

The procedure of sample preparation included: grinding, sieving, weighting, pressing, polishing, etc. In our studies, COPR samples and the calibration standards were ground to a size smaller than 80 microns and pressed into disks using hydraulic press at 24,000psi.

Ten XRF standards were prepared from certified standards of known compositions. The GXR-2 and GXR-3 are standards purchased from United States Geological Survey (USGS). The San Joaquin (SJ) standards are from National Institute of Standards and Technology (NIST). The other standards are prepared by the commercially available standards and pure metal oxides.

The certified standards were mixed with other pure chemical compounds, Fe_2O_3, Cr_2O_3, $CaCO_3$, MgO, and Al_2O_3 to obtain the desired standard concentrations (Kamolpornwijit 2000).

To minimize the particle size effect and level the surface, the standards are thoroughly mixed with additive and pressed into an aluminum cup at a pressure of 24,000psi (**Figure 3**). Each pressed disk is prepared from 5.3 gm of standard and 1.7 gm of spectroblend®. Ten standards were prepared and calibrated under the vacuum environment. The concentrations of standards are shown in **Table 5**.

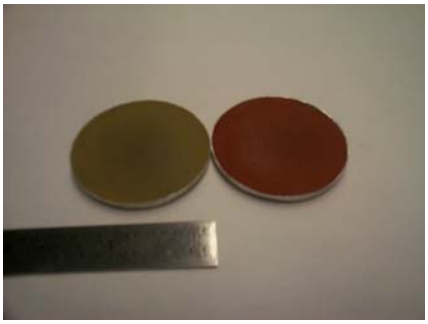

Figure 3 XRF Standards: Low (Left) and High (Right) Iron Content

Table 5 Compositions of Certified and XRF Standards by Weight

	Fe2O3	Cr2O3	CaO	SiO2	Al2O3	MgO	Na2O	K2O	MnO	P2O5
GXR3	27.180	0.000	19.000	13.360	12.100	1.340	1.130	0.880	2.880	0.250
SJ	5.000	0.000	2.640	63.450	14.170	2.500	1.560	2.450	0.010	0.140
std1	42.949	14.700	10.450	7.348	6.655	2.697	0.622	0.484	1.584	0.138
std2	38.790	11.760	12.407	9.218	6.617	4.690	0.627	0.538	1.440	0.131
std3	27.881	9.800	14.497	14.261	7.287	7.788	0.711	0.715	1.297	0.131
std4	16.701	5.880	18.584	21.473	6.892	9.853	0.712	0.913	0.665	0.098
std5	12.533	2.940	22.018	27.117	7.241	5.094	0.771	1.094	0.378	0.089
std6	7.487	1.960	24.441	30.990	7.286	3.214	0.794	1.211	0.120	0.077
std7	1.750	0.000	37.347	22.208	4.960	0.875	0.546	0.858	0.004	0.049
std8	4.200	0.980	10.623	53.298	11.903	2.100	1.310	2.058	0.008	0.118
std9	7.577	4.900	4.698	46.419	21.734	1.951	1.262	1.847	0.439	0.136
std10	2.750	0.000	26.668	34.898	7.794	1.375	0.858	1.348	0.006	0.077

The characteristic x-ray of element is hardly affected by its oxidation state and this allows XRF to analyze any sample against the standard of different phases. The characteristic x-ray

fluorescence has less energy than the incident x-ray, and therefore x-ray fluorescence does not penetrate the sample as deeply as the incident x-ray. The largest thickness of the sample that characteristic x-rays can penetrate is called penetration depth. Due to the limited penetration depth, the particle size has a very strong influence on the analysis when the matrix is heterogeneous. A system with non-uniform distribution of elements gives different results at different orientations. The effect is aggravated if the particle size is larger than the penetration depth. The reduction of particle size helps alleviate both the particle size effect and the heterogeneity of COPR. Preparing samples into a pressed disk also improves the accuracy of the analysis. The surface of the pressed sample is smoother and it provides less void space than the loose sample.

Wet Chemical Analysis

The solid samples, XRF standards and COPR samples were digested in concentrated HNO3 in CEM MDS-2100 Microwave Digestion Oven, following EPA method. The resulting solutions were analyzed using the Agilent 7500i Benchtop Inductively Coupled Plasma-Mass Spectrometer System (ICP-MS), an instrument available in the Material Characterization Laboratory of NJIT, following EPA method 6020 (Inductively coupled-mass spectrometry) and Method 200.8, (determination of trace elements in waters and wastes by inductively coupled-mass spectrometry).

In order to analyze metals concentration in COPR using combined analytical methods, the solid sample (e.g., soil, sewage sludge, mixed waste, oil, plastics, metals and alloys, rocks, etc.) should be digested into solution prior to analyzing. Wet digestion is a classical technique that requires complex mixtures of acids for sample decomposition. Microwave digestion is a convenient and timesaving closed-vessel method compared to the traditional approach of open beakers on hot plates. Samples are digested for metals analysis in sealed TFE-lined bombs placed in a microwave oven. Once a solid sample has been digested in CEM MDS-2100 Microwave Digestion Oven, the resulting solution can be analyzed using one of Agilent 7500i Benchtop ICP-MS instruments available in the Material Characterization Laboratory.

X-Ray Diffraction Spectrometer (XRD)

The Philips XRD, X'Pert XRD, was used to investigate phase assemblages of the sample. The incident x-ray Cu$k\alpha$ is diffracted by the sample of different phases from 5-70 2θ angles with a

step size of 0.01°. Samples were ground to smaller than 80 microns and placed in inverse sample holders in such a way to minimize preferred orientation.

The XRD is accompanied by a software package (Philips's reduced database-PDF1) containing diffraction patterns of over 80,000 compounds prepared by the International Centers for Diffraction Data (ICDD). The series of diffracted angles from the sample is then identified against standard patterns in the database. Though the searching for the matching pattern is automatically done, the identification is done manually by comparing the match in terms of the diffracted angles and relative intensity.

The XRD is powerful and versatile nondestructive analytical techniques for the identification and quantitative determination of crystalline solid phases (atomic arrangements) within solid and powdered samples. In fact, it is the only technique that can distinguish between phases. The incident x-ray, Cukα, is diffracted by the sample of different phases, or same phase but different orientations, at different angles. The diffracted angles relate to the d-spacings, the crystal lattice parameters of a unit structure according to Bragg's law. In this report, the incident x-ray Cu$k\alpha$ is diffracted by the sample of different phases from 5-70 2θ angles with a step size of 0.01°.

The particle size is also critical for the diffraction analysis. It has to be sufficiently fine so that all d-spacing values have the same chance to orient perpendicularly to the sample surface. The preferred orientation occurs when certain orientations appear too frequent. In our experiment, samples were ground to smaller than 75 microns and placed in inverse sample holders in such a way to minimize preferred orientation.

Scanning Electron Microscope (SEM) with Energy Dispersive X-ray (EDX) Detector

Scanning electron microscope (SEM) with Energy Dispersive X-ray (EDX) detector was used for the morphology studies and analysis of local composition of the reaction mixtures after TGA experiments. The SEM is LEO 1530 VP FE-SEM. The EDX is from Oxford instrument with INCA software.

In SEM, the bombardment of electron beam on the sample causes the emission of secondary or back-scattered electrons and X-rays. Back-scattered electrons carry compositional information of samples. Heavy atoms or atoms with high atomic numbers have higher scattering than lighter ones, thus back-scattered images contain compositional information, i.e. the brighter the

area the heavier the elements contained within the area. All the presented SEM images are captured using back-scattered electron detector. Equipped with the EDX, SEM also allows the study of the sample composition. The EDX is in fact the x-ray detector capturing all characteristic x-rays and separating them by their energies; so-called Energy Dispersive X-ray fluorescence spectrometer. The EDX software, called micro-mapping, allows the quantitative study, if calibrated, of the elemental distribution. The EDX, in this research, gives semi-quantitative results since it is calibrated against the instrument software and not a prepared set of standards.

TGA Analysis

The reduction study was performed in a Thermo-Gravimetric Analyzer (TGA, Perkin-Elmer, model TGA7), where samples were flushed with nitrogen to create an oxygen-free environment. The preliminary reduction study was conducted using COPR from NJDEP Site 115 South End (Sample 2-S) as a representative COPR sample. The particle size of COPR used was smaller than 100 mesh. Unless otherwise stated, the carbon content for reduction is 15% weight relative to the COPR. The standard TGA test condition was 3-hour flushing with nitrogen at a rate of 100 ml/min at 1 atm and room temperature, then ramping at a rate of 40°C/min to a set temperature (1500°C) with N_2 flushing rate at 20 ml/min, maintaining in isothermal state for 1 hr, and cooling at a rate of 20°C/min down to room temperature.

COPR sample weighing less than 50mg was placed in a graphite crucible which was then placed on a standard platinum pan for TGA experiments. Different amounts of sand were added to adjust the chemical composition of the COPR.

Bench Scale Melting

The metal oxides reduction and separation at a fine scale was achievable under the TGA environment. The results from ESEM and EDX suggested clean metal separation where Fe and Cr were concentrated within metal phase along with Si. The slag phase contained mainly Ca, Si, Al, and Mg with very low concentrations of Fe and Cr. The promising result from the fine scale experiment encouraged further experiment at a larger scale.

The bench scale experiment was conducted using box furnace, CM model 1710FL. The heating chamber is 12”x12”x12” in dimension, with a gas port allowing flushing of inert N_2 gas. The maximum operating temperature is 1700°C. The controller allows heating, holding, and cooling in various stepwise combinations. The flushing of inert gas (N_2) is required to minimize

oxidation of both graphite crucible and powder graphite by oxygen remaining within the heating chamber.

The crucible used in this experiment was a graphite crucible, Galloni 3013, 2.285" outside diameter x 1.415"inside diameter x 3.05"depth, since it provides additional reducing agent and minimizes oxide contamination associated with the use of alumina crucibles.

Melting Recipe: Iron oxide reduction by carbonaceous compounds proceeds at temperatures as low as 700°C depending on the partial pressure of oxygen. It is possible that the reduction is completed before the slag or metal begins to melt. The study of slag behavior thus may be simplified by excluding readily reduced metal oxides from its initial composition. The modified compositions of COPRs excluding iron and chromium oxides are given in Table 6. The high calcium concentrations in COPRs rendered the high basicity, 2.7-8.3, **Table 6**. The liquidus temperatures of modified COPRs were as high as 2000°C, **Table 6**. By neutralizing COPRs with sand (SiO_2), the liquidus temperature decreased to less than 1400°C. Note that the percentage of sand addition was based on the mass of initial COPRs. The liquidus temperatures were taken from the ternary phase diagrams, CaO-SiO_2-MgO, with constant concentrations of Al_2O_3. The phase diagrams were available at an increment of 5% Al_2O_3 hence the liquidus temperatures were taken from the diagram with the nearest Al_2O_3 concentration to COPRs.

Table 6 Composition amendment and liquidus temperature.

COPRs	Sand addition (% of initial COPR mass)	Composition (% weight) Al_2O_3	CaO	MgO	SiO_2	Basicity (mole/mole) $\frac{CaO+MgO}{Al_2O_3+SiO_2}$	Approx. liquidus temp C
Initial composition including Fe_2O_3 and Cr_2O_3							
CD		9.5	28.0	11.8	12.0	2.7	
South		7.4	35.3	11.3	5.1	5.8	
North		5.7	47.0	9.2	4.4	8.3	
Modified composition excluding Fe_2O_3 and Cr_2O_3 and normalizing to 100%							
CD		15.5	45.7	19.2	19.5	2.7	~1950
South		12.5	59.8	19.2	8.6	5.8	~2000
North		8.5	70.9	13.9	6.6	8.3	~2000
Final composition after sand addition to neutralize basicity							
CD	30.6	10.4	30.7	12.9	46.0	1.0	~1350
South	47.3	6.9	33.2	10.6	49.2	1.0	~1300-1400
North	59.7	4.5	37.3	7.3	50.9	1.0	~1400

Carbon Addition: Stoichiometric reduction of Fe_2O_3, Fe_3O_4, and FeO to Fe metal and CO_2 requires 11.3, 10.5, and 8.5% carbon by weight, respectively. During TGA experiment approximately 15% by weight of carbon was added to account for potential oxidation by O_2 remaining in the heating chamber. At this carbon concentration the reduction was complete and there was a clear metal separation. For the bench scale experiment, a higher percentage of carbon, 25%, was used to account for the excess oxygen in the heating chamber of the incompletely sealed furnace.

Heating program: Unless otherwise noted, the heating program started by heating the furnace to 100°C, holding for 2 hrs during which N_2 was flushed through the heating chamber, ramping to 1500°C within 45 minutes, holding at 1500°C for 1-2 hrs, then cooling to room temperature.

Results and Discussion

Sample Characterization

X-ray Fluorescence Spectrometer (XRF): The COPR samples were grounded to smaller than 80 microns and prepared in exactly the same way as the standards. The samples were rich in calcium, iron, silica, alumina, magnesium, and chromium as analyzed by XRF (**Table 7**).

Calcium oxide concentrations are as high as 29-46% by weight. If calcium present in COPR mainly as $CaCO_3$ or $Ca(OH)_2$, its weight percentage would be higher than 50%. The high calcium concentration is expected as a result of lime addition during chromate extraction process. With low concentration of SiO_2 and Al_2O_3, the COPR is believed to be disposed of as-is with little degree of mixing with indigenous soil.

Table 7 Chemical Compositions of three COPR Samples by XRF

	Fe_2O_3	Cr_2O_3	CaO	SiO_2	MgO	Al_2O_3	Na_2O	K_2O	MnO	P_2O_5
Sample-1	15.99	2.96	29.95	12.08	11.66	9.46	0.47	0.26	0.11	0.04
Sample-2S	15.71	3.71	35.39	5.16	11.42	7.47	0.36	0.04	0.10	0.02
Sample-2N	9.249	2.46	46.83	4.43	9.24	5.67	0.22	0.07	0.08	0.02

Iron oxide concentrations, reported as Fe_2O_3, are 9-16%. The molar ratio (Cr/Fe) is 0.18-0.25, which fall within the Cr/Fe ratio for stainless steel. Iron oxide concentrations from these 3 sites

are not as high as iron oxides in some COPR from other sites (Kamolpornwijit, 2000); however, the ratio of Cr/Fe is similar.

As a reference, from previous samples from 9 sites, the ranges of weight percentages by conversion are: calcium carbonate (11.6-58.2%), silica (7.4-48.9%), alumina (10.4-15.9%), and iron oxide (10.7-33.1%), magnesium oxide (3.1-10.5%) and chromium oxide (1.5-10.7%).

Inductively Coupled Plasma-Mass Spectrometry (ICP-MS): Wet Chemical Analyses were performed to check the accuracy of XRF measurements (**Table 8**). Concentrated nitric acid was used for the microwave digestion. No attempt was made to digest Si using hydrofluoric acid for Si analysis.

Table 8 Comparison of Metal Composition by ICP-MS and XRF (mg/g)

		Na	**Mg**	**Al**	**K**	**Ca**	**Cr**	**Mn**	**Fe**
Sample 1	ICP-MS	1.60	26.83	29.73	19.00	91.68	14.28	0.88	68.20
	XRF	2.62	50.30	37.90	16.40	150.11	15.34	0.66	84.75
Sample 2N	ICP-MS	0.85	24.62	17.85	0.14	184.20	11.53	0.63	38.19
	XRF	1.21	42.01	22.75	0.41	253.22	12.72	0.45	49.03
Sample 2S	ICP-MS	2.18	27.20	32.12	0.08	135.39	19.18	0.84	75.88
	XRF	2.01	52.04	29.82	0.27	151.15	19.23	0.56	83.30

Generally, Na, K, and Mn are the minor elements in COPR samples and XRF standards, and they produced similar chemical composition results from the ICP and XRF analyses. The mineral phases of COPR samples are easier to digest, and ICP and XRF results are quite consistent with each other. Some ICP-MS measurements gave lower concentrations (for example, the chromium content) for XRF standards. The discrepancy might be due to the incomplete digestion, which is under further investigation. The large particle size and high concentration of metals might also reduce the on the microwave digestion efficiency.

The Cr concentration from both XRF and ICP-MS are comparable when the difference is less than 10%. The differences in Fe concentration are higher, between 9-25%. The differences in other elements are quite high, as high as 66%. In general, the concentrations estimated from XRF are higher than those from ICP-MS. Both instruments are known for their accuracy and

precision, hence we would assume that most of the differences to come from the sample heterogeneity and the digestion:

1. Microwave digestion is not applicable to Si analysis. It is possible that certain elements associated with Si might not be completely digested.
2. Different phases, i.e. calcium oxide versus calcium silicate hydrate, may be subjected to different degrees of dissolution by HNO_3.
3. The very high concentration of some elements, i.e. iron oxide and calcium oxide, might result in incomplete dissolution.
4. The presence of spectroblend® in the sample is digested. The spectral blend may cause excessive vapor formation during digestion.

The cause of discrepancy is not known. Since the incomplete digestion may be the cause of major discrepancy in metal analysis, we propose use of XRF as a tool for bulk chemical analysis.

X-Ray Diffraction Spectrometer (XRD): **Figure 4** shows XRD diffractograms of COPR for all three samples (1, 2-S and 2-N). The phase identification in COPR is often not conclusive due to the heterogeneity of COPR. It is not possible to identify all phases present in COPR. Some major phases that can be identified with confidence include $CaCO_3$ (or $MgCO_3$), $Ca_2(Fe_{2-x}Al_x)O_5$ (brownmillerite), $Ca(OH)_2$ and SiO_2.

While previous XRD studies on nine sites in Hudson County shows the major phase for iron and chromium is Spinel (Mg, Fe).(Fe, Cr, $Al)_2O_3$, the XRD pattern of these 3 samples indicates the major phase for Fe content is brownmillerite, $Ca_2(Fe_{2-x}Al_x)O_5$. Also in the two samples supplied by Honeywell, significant peaks of $Ca(OH)_2$ (portlandite) were observed, along with that from $Ca(Mg)CO_3$ (calcite). The XRF results also showed a very large amount of Ca content (~46% weight in the form of CaO). These results are consistent with the fact that high weight percentage of calcium was added during the chromate extraction process.

There were large amounts of white pellets, which were well separated from the grey or slightly greenish COPR, from samples 2N and 2S. Analysis of the white pellets by XRD (mineral phase determination) and XRF (chemical composition analysis) revealed the major phase as $Ca(OH)_2$. This finding can account for the large content of Ca in both samples, although the significant amounts of $Ca(OH)_2$ was not seen in our previous studies on other nine sites in Hudson County. The source of Si largely comes from SiO_2 (quartz).

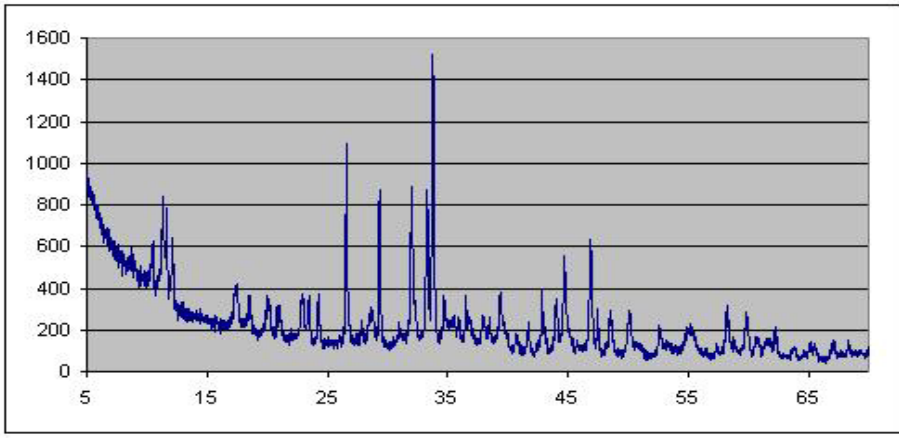

(a)

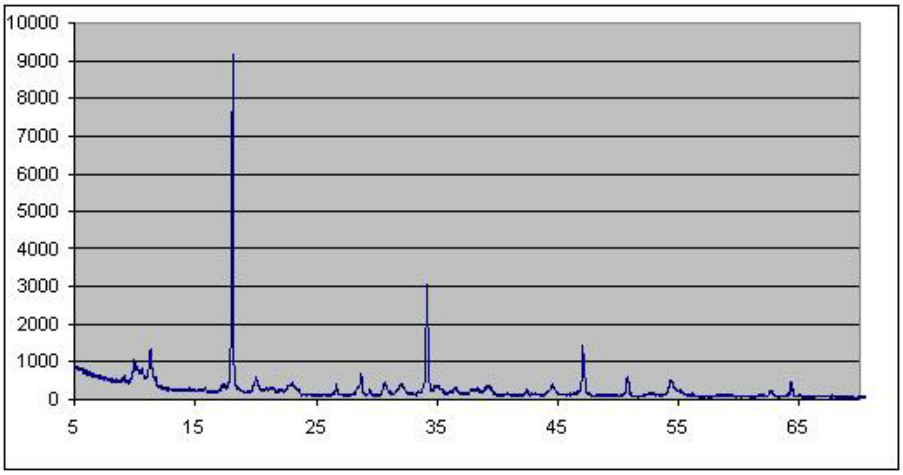

(b)

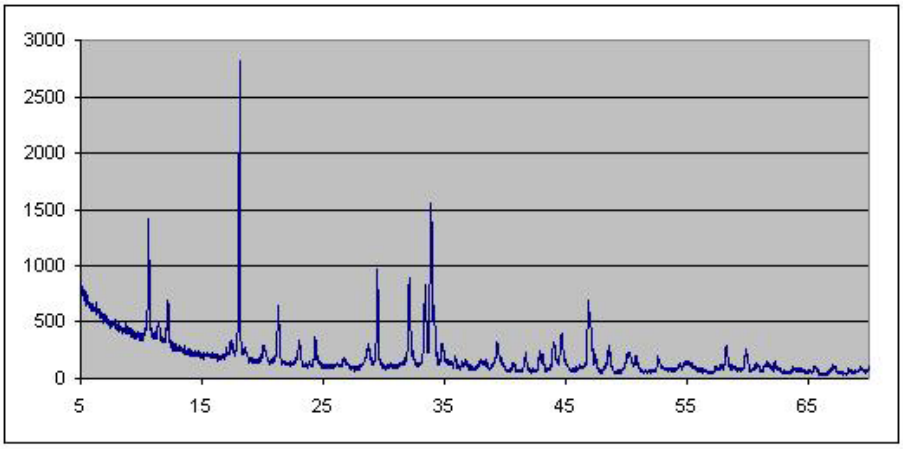

(c)

Figure 4 XRD Diffractograms of Samples 1 (a), 2-S (b) and 2-N

The Cr content is relatively small (2-4% weight in the form of Cr_2O_3 by XRF). The minor minerals containing Cr is identified as $Mg_6(Al,Cr,Fe)_2(CO_3)(OH)_{16}\bullet 4H_2O$ (hydrotalcite), and $Mg_5(Al,Cr,Fe)(Si_3Al)O_{18}H_{18}$ (Cr-Clinochlore). The existence of hexavalent chromium in COPR is a concern, but the phase of hexavalent chromium could not be identified along with other major phases due to its low concentrations. $CaCrO_4$ (calcium chromate) could be a possible mineral phase for chromium, although its peaks overlap with brownmillerite which is one of the most dominant phase in the COPR. The existence of $CaCrO_4$ had been confirmed previously in our group. Water extraction and filtration was utilized to extract chromate from CD (Colony Diner). The filtrate was yellowish and was allowed to dry in an oven at 100°C. The precipitate was subsequently identified using XRD as calcium carbonate and $CaCrO_4.2H_2O$ (chromatite hydrate).

TGA Reduction Study

When heated samples go through phase transitions, metal oxides are potentially reduced if carbon is added. The weight loss pattern from TGA is complex, reflecting the heterogeneity nature of samples. We attempted to assign weight loss at different temperatures to certain mechanisms based on both our experimental study and literature search. The results along with discussion are presented below. The reduced sample after TGA experiment was further investigated using SEM equipped with EDX to verify the metal formation and separation.

Oxidation of Graphite Crucible: Under the TGA experiment, samples are continually purged with nitrogen to remove oxygen within heating chamber thus eliminating unnecessary oxidation of graphite crucibles. During the preliminary test, the graphite crucibles were completely oxidized when the heating chamber was not sealed well. The furnace chamber was flushed with nitrogen at a rate of 100 CC/min for 2 hours before heating up to the desired temperature for the isothermal period. It shows that under standard operation conditions, as described in Experimental section for metal oxide reduction, approximately 3 mg weight loss can be attributed to carbon weight loss.

Reduction of $CaCO_3$: Calcium carbonate is abundant in all COPR samples. It started losing its CO_2 around 700°C; the reduction was complete at 950°C, (see **Figure 5).** At temperatures higher than 950°C there was no observable weight loss confirming the stability of CaO at 1400°C.

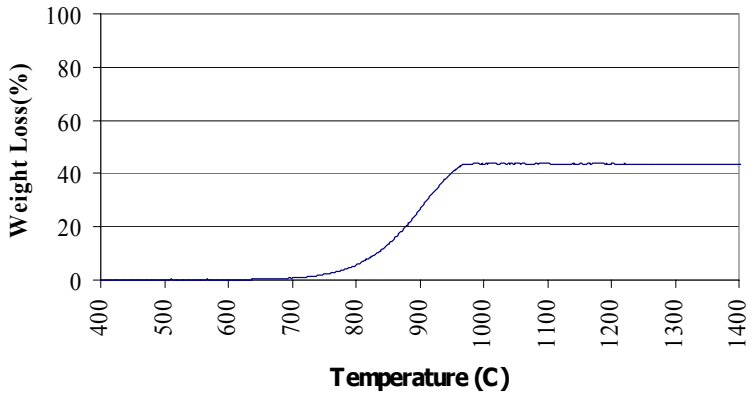

Figure 5 The results from TGA, the Reduction of $CaCO_3$ (Kamolpornwijit, 2000).

Metal Oxide Reduction of COPR: Sample-2S was used in this preliminary study of metal oxide reduction and metal separation by TGA experiments. Fine carbon powder (15% wt. of the COPR) was used as the reductant. Weight loss curves and the variation of weight differences with temperature are shown in **Figure 6**. The peaks in Figure 3b represented weight losses from moistures and organic parts, in samples at 150~400°C, from $CaCO_3$ at ~650°C, and from metal oxide at 1000~1400°C. Weight losses increased drastically above 1000°C.

In **Figure 6b** there are two peaks in the range of 1000-1400°C. It might imply that an easily reduced fraction first went through reduction, followed by the reduction of relatively more stable fraction. Ignoring other factors, the stability of oxides is in the order of SiO_2> Cr_2O_3> FeO> Fe_3O_4> Fe_2O_3. Hence the highly reducible types, Fe_3O_4 and Fe_2O_3, were first reduced to FeO around 1000°C. At 1100°C, FeO was reduced to metal. Cr_2O_3 and some amount of SiO_2 can be reduced to respective metals at higher temperatures.

The weight difference peaks also implied that the reduction of iron oxide proceeded very fast and readily finished before the isothermal period above 1400°C. Previous studies and literatures suggested the reduction of chromium oxide (which is in smaller amount than iron oxide) occurred around 1400°C. The reduction of some SiO_2 to Si in the isothermal step of high temperature has also been reported and confirmed by the EDX results which will be discussed later in this report. The reaction mixtures yielded mostly dust and some glasslike droplets. There was neither the metal separation nor the presence of tiny shiny specks. Hence, the metal separation was not achievable without sand addition as confirmed in our previous literature search due to highly basic nature of the COPR with excess calcium.

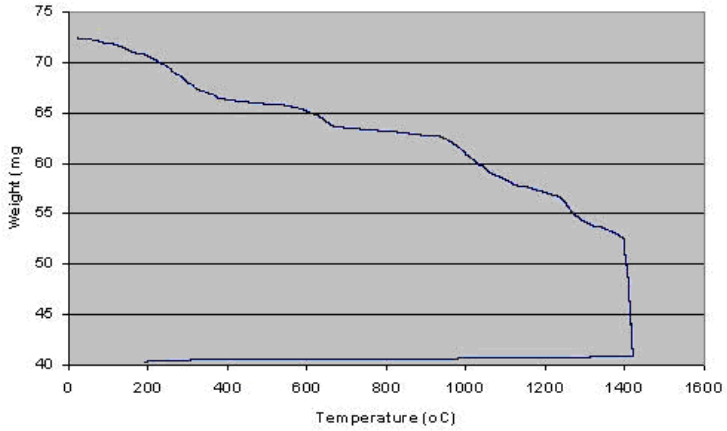

(a)

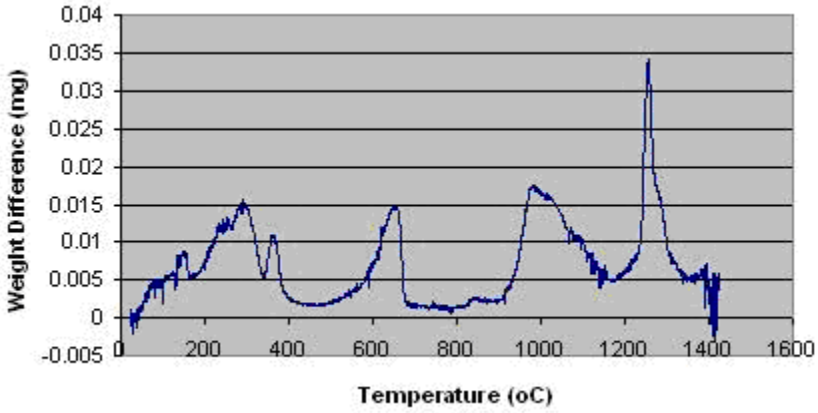

(b)

Figure 6 The results from TGA without sand (a) Weight Loss Curve and (b) Weight difference.

Metal Separation: The reduction of iron oxide is very rapid; therefore the limiting step for the iron droplet formation would depend on the grain growth and metal separation. Metal separation is easier in the liquid state. It is proposed that metal separation could be achieved by adjusting the composition of COPR to melt at a low temperature and have low viscosity. The solid state diffusion of acidic and basic oxides at high temperatures may yield intermediate compounds with lower melting temperatures, and subsequently melt and form a liquid pool to which the high melting temperature compounds can be further dissolved.

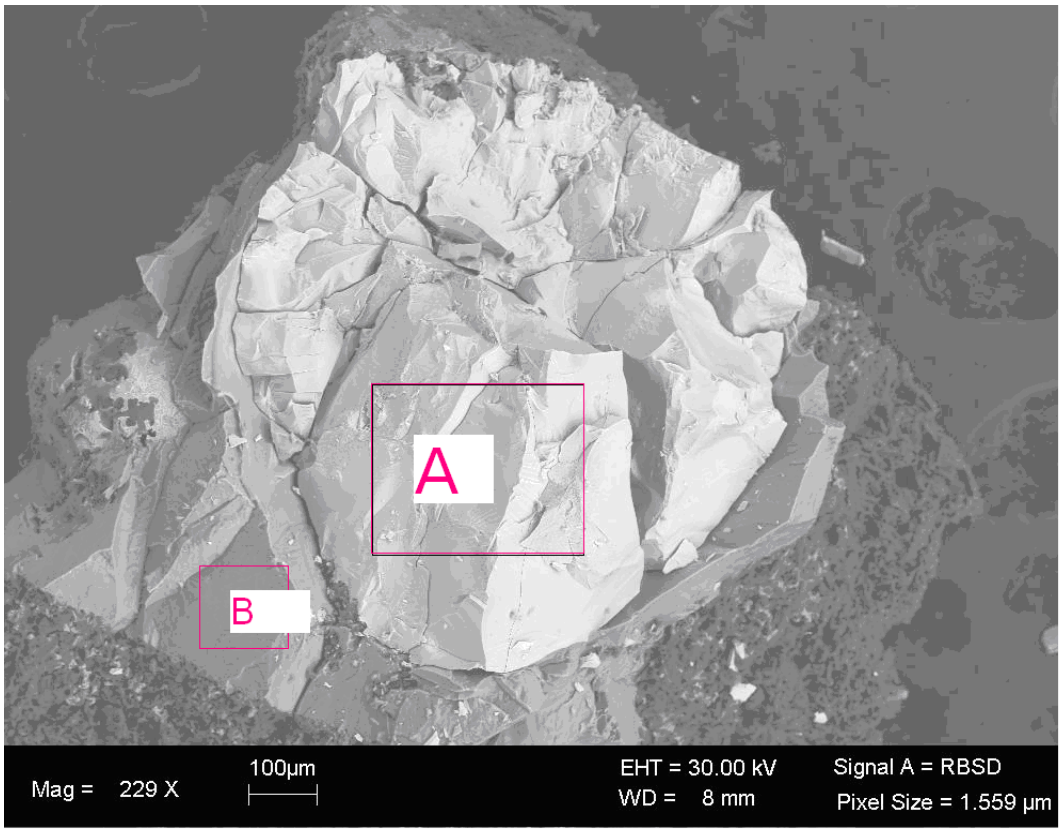

(a)

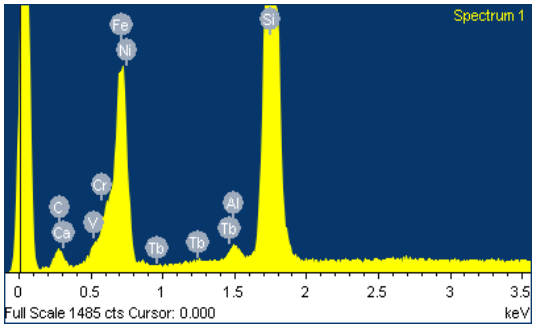

EDX data for Region A

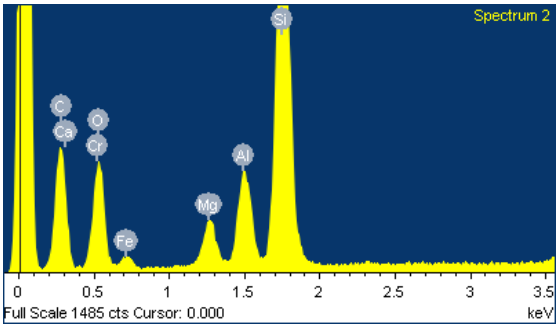

EXD data for Region B

(b)

Figure 7 The SEM (a) and EDX (b) results showing the separation of metal phase (Region A) and oxide phase (Region B)

TGA experiments had been performed on COPR sample 2S and 15% carbon, with different amount of sand addition. The addition of sand, an acid oxide to COPR rich with CaO, a basic oxide, should bring the melting temperature down and ease the agglomeration of the metallic

iron. With 50% sand addition, some shiny metal ball was obtained in the product resulted after melting, as shown the SEM-EDX results from morphology studies (**Figure 7**).

Table 9 EDX chemical composition results for Region A and B of SEM Figure 4

Elements	A		B	
	Weight %	**Atomic%**	**Weight %**	**Atomic%**
Fe	50.81	28.11	3.63	1.07
Cr	6.03	3.58	0.81	0.26
Si	24.23	26.66	9.37	5.50
Ca	0.23	0.18	11.32	4.66
C	15.42	39.67	37.70	51.78
O	nd	nd	33.12	34.15
Al	0.88	1.00	2.40	1.47
Mg	nd	nd	1.64	1.11

Note: nd none detected

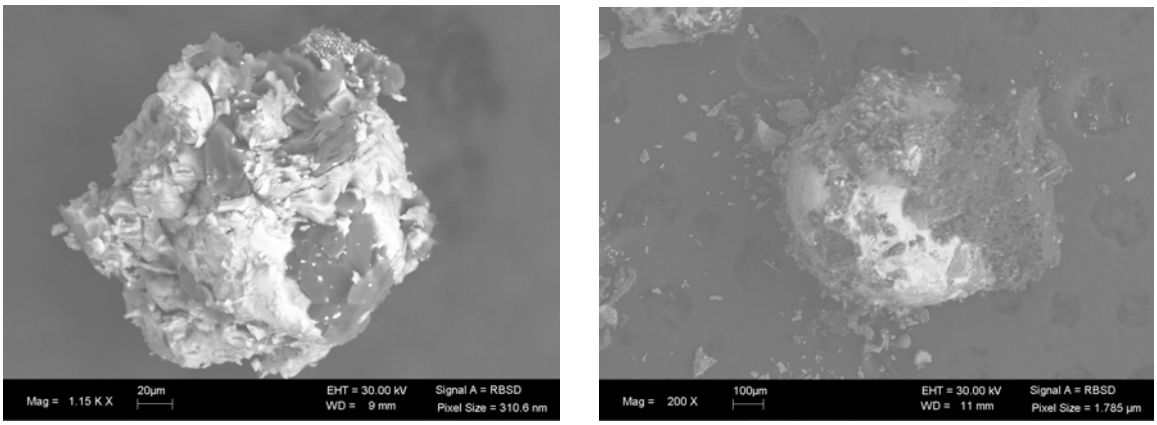

(a) (b)

Figure 8 The SEM pictures of no metal separation at 20% sand addition (a) and a metal ball with 40% sand addition (b) to sample 2S

Table 9 shows the composition of the metal phase (Region A), which was mainly Fe (28.1%) and Cr (3.6%). The EDX showed no oxygen in this phase indicating oxides were not detectable. The Region B which was attached to the graphite crucible had other major elements; their oxides including metal silica from the reduction of SiO_2 and carbon. It also had

small concentrations of Fe and Cr. The factors governing the metal separation include, but are not limited to, the melting temperature and the slag viscosity which depend on slag compositions. The behavior of slag or oxide systems can be partly described through phase diagrams. The slag components of interest are CaO, MgO, SiO_2, and Al_2O_3. **Figure 8** shows a picture of metal ball with the addition of sand to COPR Sample 2S. Preliminary data suggests the feasibility of metal separation with 40% sand addition for COPR Sample 2S, but no metal separation below 20% sand addition. Future systematic studies will use phase diagram of quaternary system CaO-MgO-SiO_2-Al_2O_3 because phase diagrams provide information on thermodynamically stable states, i.e. as liquid or liquid in equilibrium with solids, depending on the sample compositions.

Bench Scale Melting

With the encouraging results from TGA bench scale melting was performed using the box furnace (CM model 1710FL) flushed with Nitrogen gas. Table 10 shows the melt recipes and the melt temperatures of all samples. It lists five melting recipes. The first melt recipe mimics the positive results obtained from TGA where no metal separation was detected. Hence, we decided to increase the melting temperature and residence time in the second melt. However, this recipe also did not produce metal separation. Hence, to investigate the problem of no metal separation regent grade, iron oxide was melted in the third melt. During the third melt, the iron oxide reduced to metal, which agglomerated as tiny metal balls. In the fourth melt, the size of the sample was increased, which showed weak metal separation. Thus, during the fifth melt the carbon content was reduced. Two separate carbon contents were used. The lower carbon content melt showed strong metal separation. It was found that the carbon crucible contributed to excess carbon which prevented metal separation.

Recipe #1-Melting COPRs with 25% Carbon, Adjustment of Basicity to 1, 1500°C: The sample size was 10 gm, with 2.5 gm of C and sand addition to achieve basicity of 1, 60, 30, and 50% for North, CD, and South respectively. The melt from all 3 COPRs separated into 2 phases: light brown droplets, and dark brown fines. The droplets were not attracted to the magnet while the dark fines were. The XRD results, **Figure 9**, suggested the light brown were mixed oxides of CaO, SiO_2, MgO, and Al_2O_3. Specifically calcium silicate ($CaSiO_3$) and diopside (Ca (Mg, Fe, Al)(Si, $Al)_2O_6$ and (Ca, Mn)(Mg, Fe, Mn)Si_2O_6) are identified as major phases from North; while

gehlenite ($Ca_2Al(Al, Si)_2O_7$), akermanite ($Ca_2MgSi_2O_7$), and fayalite ($FeSiO_3$) are major phases of CD and South. The light brown droplets are considered the slag or oxide phase.

Table 10 Melt recipe and heating temperature

No.	Content	Weight (gm)	Carbon (% wt)	Sand (% wt)	Temp (°C)	Holding time (hr)
1	COPRs				1500	1
	-North	10	25	60		
	-Cd	10	25	30		
	-South	10	25	50		
2	COPRs				1600	2
	-North	10	25	60		
	-Cd	10	25	30		
	-South	10	25	50		
3	Fe_2O_3	10	25	0	1500	1
4	COPRs				1500	2
	-North	25	25	60		
	-Cd	25	25	30		
	-South	25	25	50		
5	COPRs				1570	2
	-North	25	4 and 15	60		
	-Cd	25	4 and 15	30		
	-South	25	4 and 15	50		

Carbon peaks were significant in the dark fines, which potentially rendered their dark color. Although this portion was attracted to the magnet, the XRD pattern did not suggest a clean metal reduction and separation. The XRD showed the significant inclusion of slag or oxide phase within this portion, **Figure 10**. The peaks at 45-46°(2θ) were potentially of metal peaks, which could be a combination of Fe, Fe_3Si, Fe_2MnSi, and Fe_3Mn_2Si. The XRD patterns from CD and from South were very similar. There was no attempt to fully identify the XRD data from North, nonetheless, the XRD data showed a mixture of oxides and possibly metal phases.

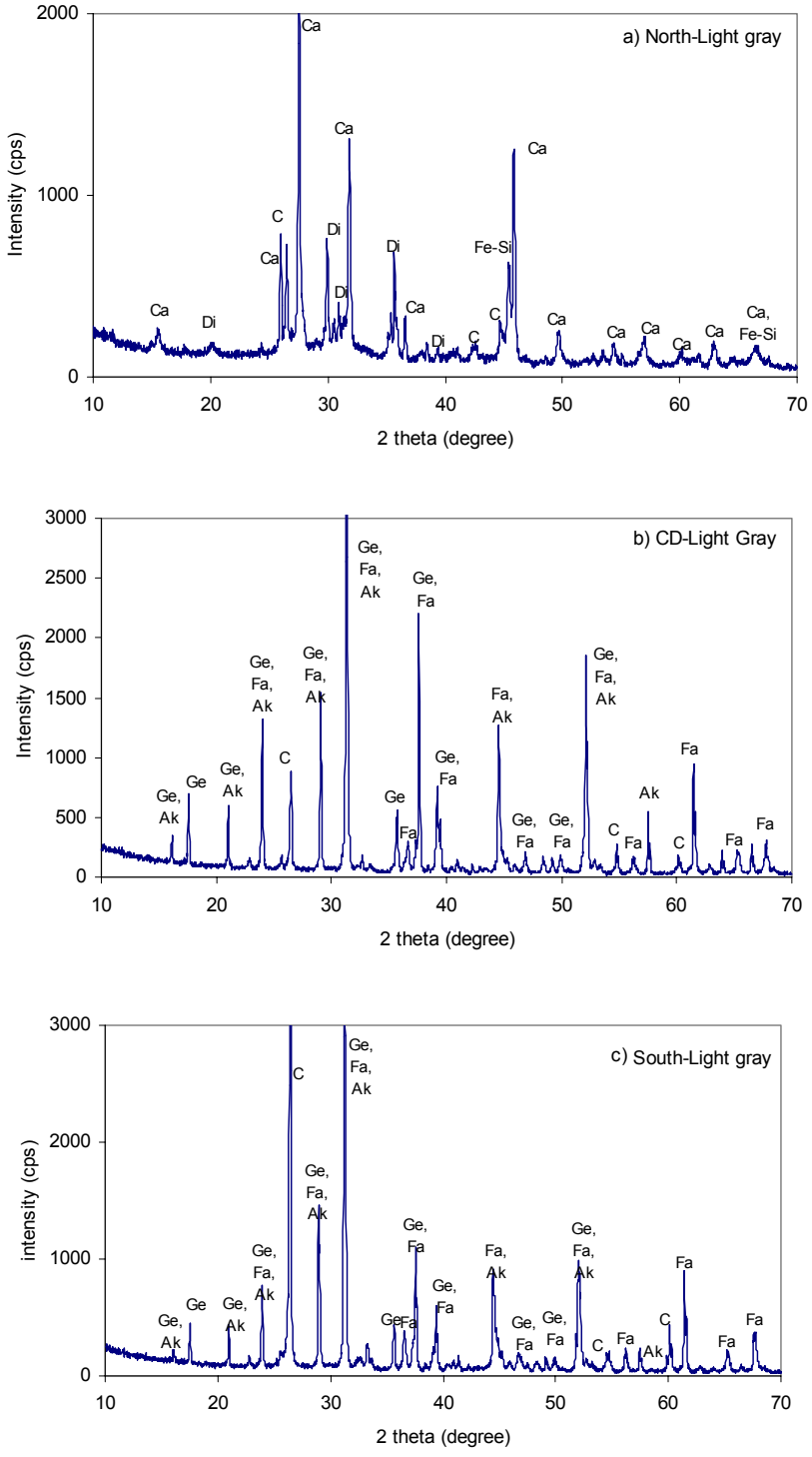

Ak : Akermanite ($Ca_2MgSi_2O_7$) Ca : calcium silicate ($CaSiO_3$)
Fa : Fayalite ($Fe_2(2SiO_4)$) Fe-Si : Fe_3Si Ge : Gehlenite ($Ca_2Al(Al, Si)_2O_7$
Di : Diopside(Ca (Mg, Fe, Al)(Si, Al)$_2O_6$ and (Ca, Mn)(Mg, Fe, Mn)Si_2O_6)

Figure 9. Diffractograms of light gray droplets from 3 sites: a) North, b) CD and c) South

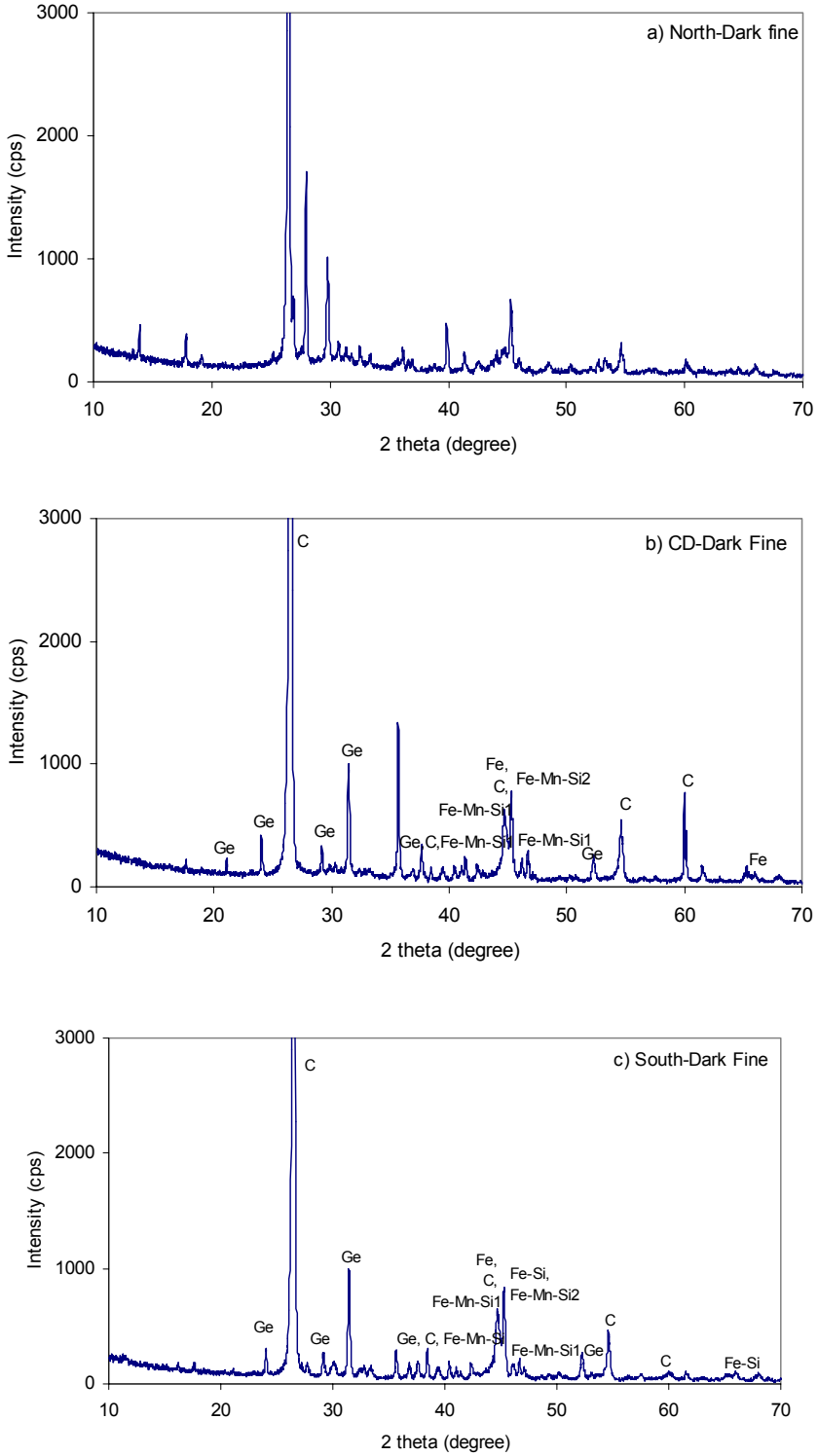

Ge : Gehlenite ($Ca_2Al(Al, Si)_2O_7$ Fe-Si : Fe_3Si C : Carbon
Fe-Mn-Si2 : Fe_2MnSi Fe-Mn-Si1 : Fe_3Mn_2Si

Figure 10. Diffractograms of dark fines from 3 sites: a) North, b) CD, and c) South

Recipe #2-Melting COPRs with 25% Carbon, Basicity = 1 at 1600°C: Given that the heating temperature was slightly higher than melting temperatures of modified COPRs, increasing heating temperature might increase fluidity of the melt thus allowing better slag and metal agglomeration. This hypothesis was the reason behind conducting the experiment at a higher temperature. Nevertheless, the results appeared to be very similar to the melting experiment at 1500°C. There were 2 phases, light gray droplets and dark fines.

Recipe #3-Melting Pure Fe_2O_3, 25%Carbon, at 1500°C:

In a heating chamber, which is not completely sealed, a complete reduction of iron oxides might not be achievable. To validate the possibility of complete metal reduction and agglomeration within this heating chamber, pure iron oxide (Fe_2O_3) was used in this part of experiment. The result suggested a reduction of most Fe_2O_3 to Fe metal, **Figure 11**. The Fe metal agglomerated into small droplets, which were strongly attracted to magnet. There was remaining carbon after melting. Although the reduction was achievable, the metal agglomeration was still localized.

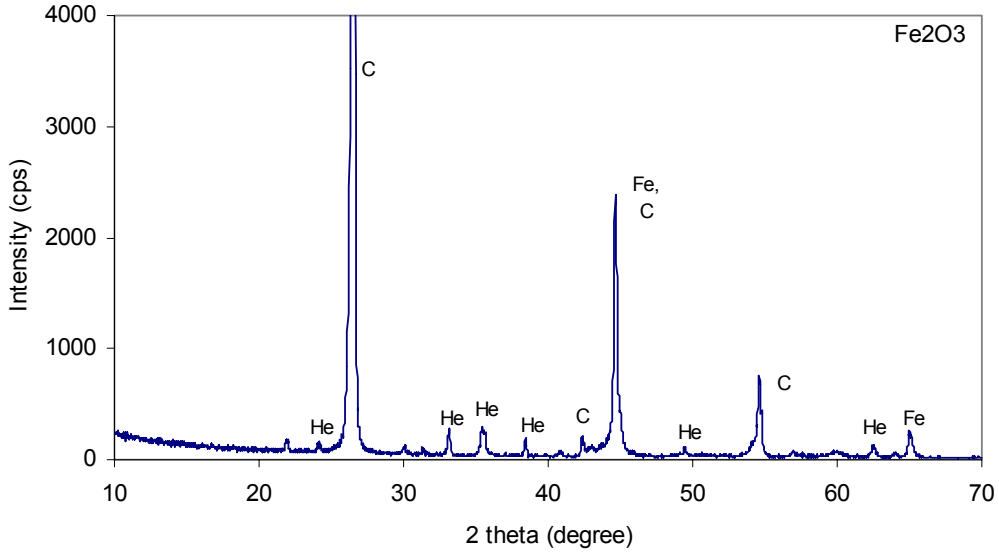

Fe : Ferrite (Fe) C : Graphite He : Hematite (Fe_2O_3)

Figure 11. Diffractogram of a melt with Fe_2O_3

Recipe #4-Melting COPRs 25% Carbon, Basicity=1 at 1570°C: Past experiments used 10 gm of sample, which was a small volume compared to the volume of crucible and the heating chamber. No agglomeration of metal might be due to the small size of sample, resulting in insufficient mass of metal. The larger mass of sample would also act as an oxygen barrier,

especially for reduction of metal oxides at the bottommost of the crucible. The density of metal is higher than of the oxides, thus metal is generally agglomerated at the bottom of the crucible. Under this hypothesis, the sample size was increased to 25 gm instead of 10 gm. At this size the sample filled over two thirds of the crucible.

The resulting melt contained droplets in different sizes and dust. Contrary to previous result, the droplets were attracted to magnet while the dust was not. The surface of droplets had a metallic shine. Upon breakage of the droplets only the thin layer of the droplet surface was attracted to magnet. The inner core had light gray color, a similar color to those droplets from past experiments. The dust was mainly carbon.

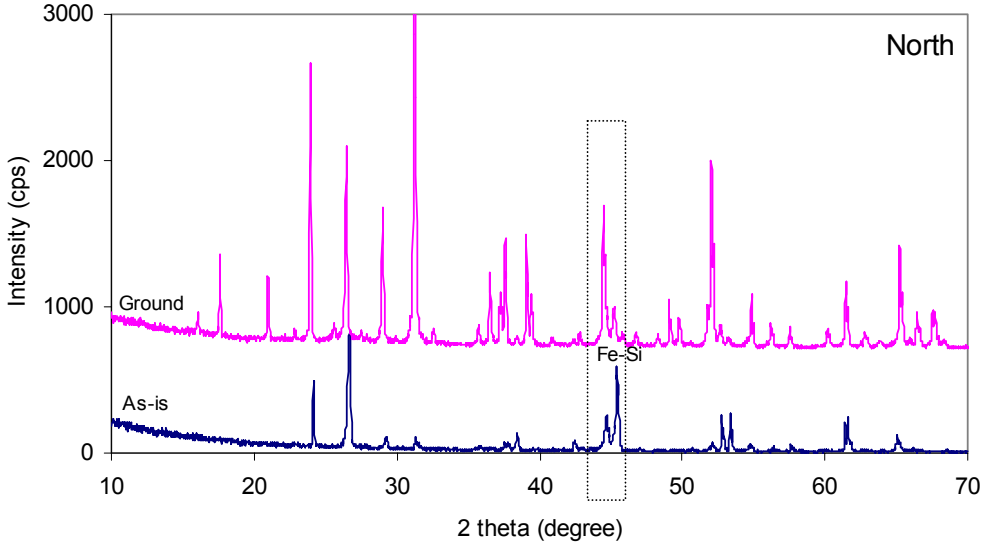

Figure 12. Comparison of diffractograms from as-is and ground samples

The XRD analysis is surface sensitive, i.e. analyzed volume is only a few microns in depth from the surface. The comparison on XRD analysis on as-is and ground droplets showed some differences, **Figure 10**. Focusing into the boxed area, there is a difference in intensity of metal peak at 46°(2θ). Note the higher intensity ratio (intensity at ~46/intensity at ~45°2θ) of metal peak in the as-is?? sample when compared to the ground sample. This suggested that metal was potentially agglomerated on the droplet surface. Nonetheless, there were many uncertainties associated with this nature of comparison. The surface of the as-is sample was not flat, resulting in both potential shift in peak position and lower intensity. The as-is sample would have strongly preferred orientation in its diffractogram. Hence, there was no attempt to

fully identify all the peaks but rather focus on differences in intensity of the metal peaks. From this experiment where metal was agglomerated on the surface of oxide droplets, it can be concluded that larger mass of samples help easing the metal reduction and agglomeration.

Recipe #5-Melting COPRs (25 gm), 4%C, Basicity =1 at 1570°C: The required carbon for complete reduction was smaller than 2% by weight of COPRs. Additionally the use of graphite crucible also provided an additional source of reducing agent. From all past experiments, the flushing rate of N_2 seemed to be sufficient to keep oxidation of crucible at a reasonably low rate. Carbon has very high melting temperatures. The excess carbon may interfere with agglomeration of metal and slag. This hypothesis was tested by varying the amounts of carbon (4 and 15%) added to COPRs.

With 4% carbon, there was a complete metal reduction, and a metal and slag agglomeration, **Figure 13**. The whole mix was melted down, resulting in 2 distinct phases: metal and slag. The metal pools accumulated at the bottom or side of the graphite crucible. The metal masses recovered from the reduction experiment were 9.56, 12.74, and 12.5% by weight for North, CD, and South respectively. The numbers represent a lower bound since the metal recovery was not complete due to the inclusion of tiny droplet in the slag. At higher contents of carbon, there was evidence of incomplete agglomeration, i.e. slag droplets on top of the slag mass.

The XRD analysis (**Figure 14**) suggested that slag from North was mainly sillimanite (Al_2SiO_5), calcium silicate ($CaSiO_3$), and diopside (Ca (Mn, Al)$(Si,Al)_2O_6$); diopside (Ca (Mn, Al)$(Si,Al)_2O_6$) and possibly mullite ($3Al_2O_3.2SiO_2$) , silica (SiO_2), and spinel ($MgAl_2O_3$) for CD slag; and melilite ($Ca_8Al_2Mg_3Si_7O_{28}$), akermanite ($Ca_2MgSi_2O_7$), and possibly gehlenite ($Ca_2Al_2SiO_7$) for South slag. All samples had a slight contamination of graphite. The slag from CD and North had a raised background at 30 degrees of 2 theta value, which was potentially due to the presence of the glass phase.

The metal phases were identified as mainly suessite (Fe_3Si) for North; iron manganese silicon ($Al_{0.3}Fe_3Si_{0.7}$) and iron manganese silicon (Fe_2MnSi) for CD and South, **Figure 15**. There was a slight possibility that all samples also contained 434-stainless steel. Although the original COPRs had Fe and Cr in a ratio similar to those in stainless steel, the presence of Si in the metal phase might interfere with the formation of stainless steel. Note that the metal sample was analyzed in the as-is sample with no grinding. Therefore, a certain degree of preferred

orientation was expected. There might also be a possibility that the metal phase on the surface which was in direct contact with slag might have slightly different phase composition from the inner core. Further characterization is necessary to precisely identify the metal phases.

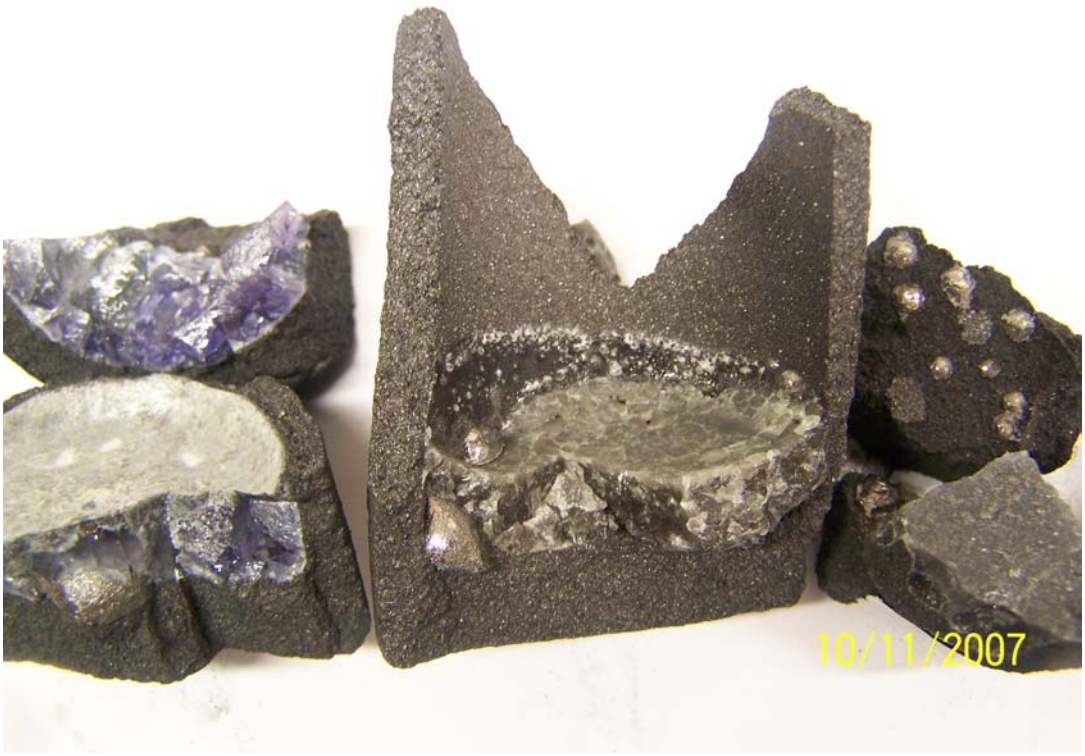

Figure 13 Melt samples from North (far left), CD (center), and South (far right)

Table 11 Composition of metal phase based on XRF analysis

	Concentration (% wt)		
Elements	CD	North	South
Mg	1.2	1.7	0.8
Al	3.0	2.3	0.9
Si	5.2	11.7	3.7
Ca	1.3	6.7	0.8
Ti	0.9	2.0	2.0
Cr	13.3	11.3	10.8
Mn	0.4	0.5	0.4
Fe	73.8	61.1	72.2
Ni	0.0	0.0	0.0

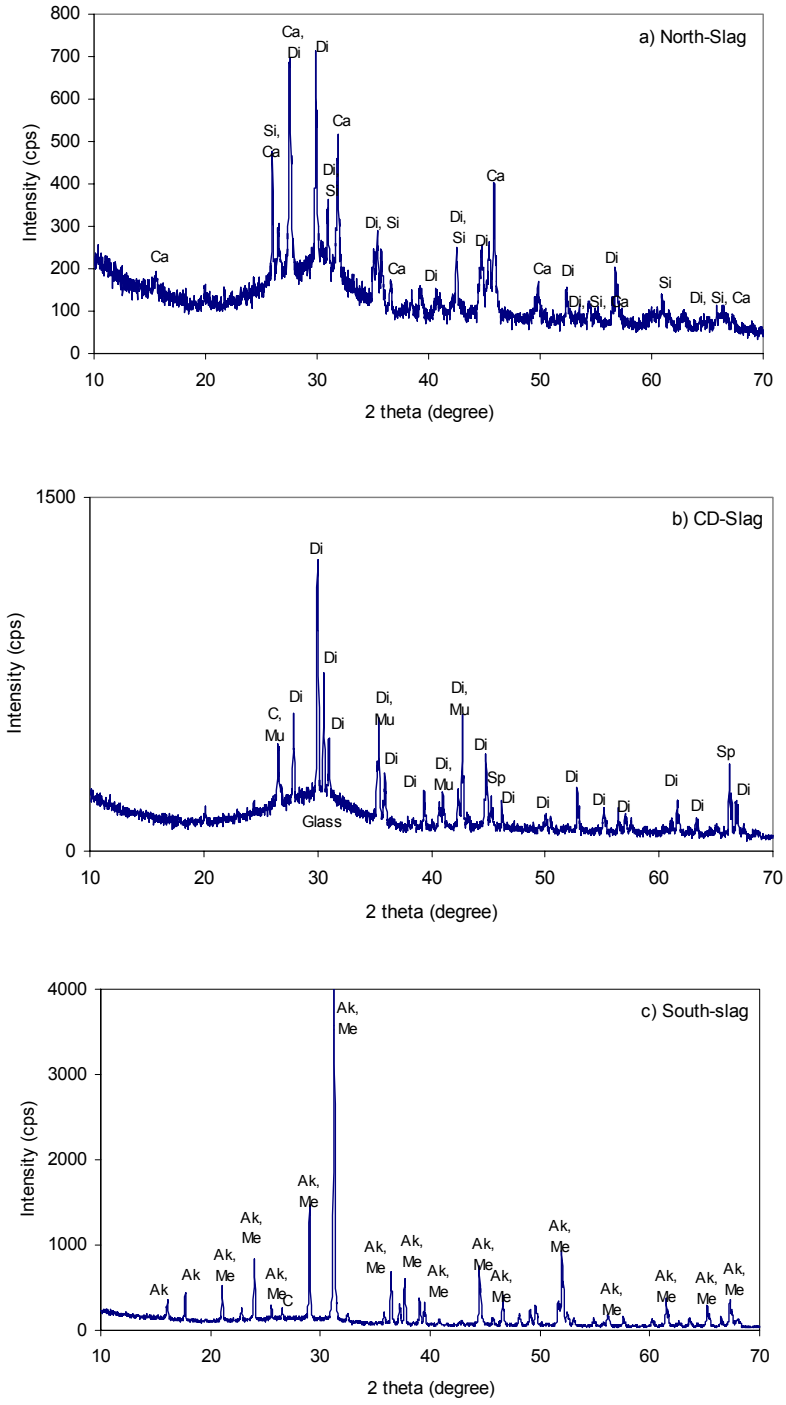

Ak : akermanite ($Ca_2MgSi_2O_7$), C : Graphite Sp : Spinel ($MgAl_2O_3$)
Me : melilite ($Ca_8Al_2Mg_3Si_7O_{28}$) Si : sillimanite (Al_2SiO_5), Mu : Mullite ($3Al_2O_3.2SiO_2$)
Ca : calcium silicate ($CaSiO_3$)
Di : Diopside (Ca (Mg, Fe, Al)(Si, Al)$_2O_6$ and (Ca, Mn)(Mg, Fe, Mn)Si_2O_6)

Figure 14 Diffratogram of slag phase from a) North, b) CD, and c) South.

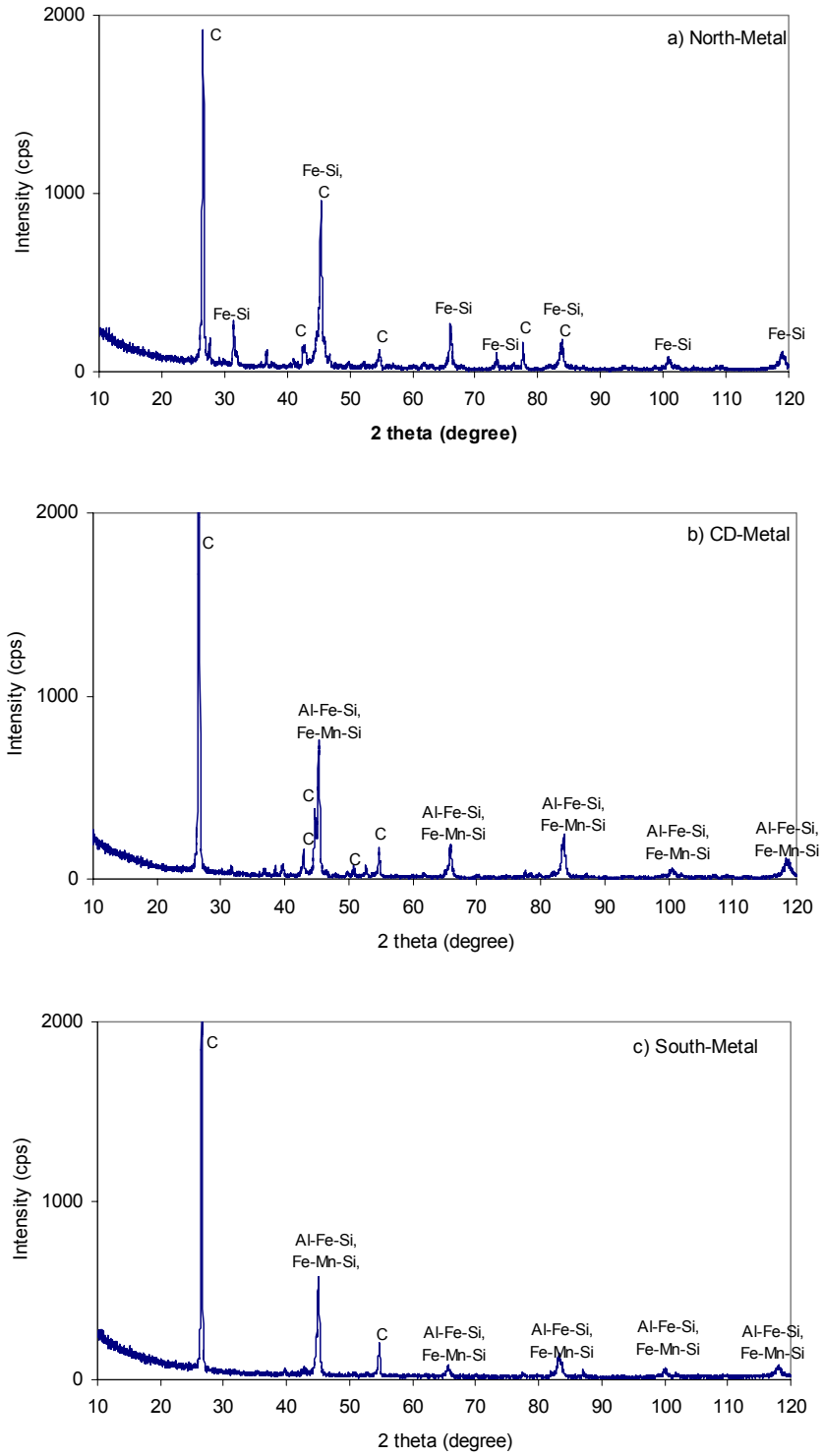

Al-Fe-Si : $Al_{0.3}Fe_3Si_{0.7}$ Fe-Mn-Si : Fe_2MnSi C : Graphite
Fe-Si : Fe_3Si C : Graphite

Figure 15 Diffartogram of metal phase from a) North, b) CD, and c) South.

The composition of metal phases was estimated semi-quantitatively using XRF. They contained high percentages of Fe, Cr, Si, Al, and Mg, **Table 11**. Factoring in the mass percentage of metal recovered from each COPR, the initial Fe content in COPRs were calculated at 9.4, 5.8, and 9.0% for North, CD, and South. The analysis of original soil has 11.13, 6.5, and 10.9% Fe for North, CD and South. These numbers are in good agreement considering the possibly incomplete recovery of metal phases.

The compositional analysis of slag based on XRF result suggested the dominant compounds are CaO and SiO_2, **Table 12**. Iron oxide was not detected while there was a low concentration of Cr_2O_3.

Table 12 Composition of slag phase based on XRF analysis

	Concentration (% wt)		
Compounds	North	CD	South
Al_2O_3	5.45	8.45	6.81
CaO	44.21	39.66	42.26
Cr_2O_3	0.19	0.06	0.28
Fe_2O_3	ND	ND	ND
MgO	5.19	10.98	7.90
SiO_2	44.99	41.01	42.68
MnO	ND	0.01	0.03
K_2O	0.11	0.14	0.09
Na_2O	0.30	0.35	0.33
P_2O_5	0.03	0.03	0.03

Summary and Conclusions

Three COPR samples from Jersey City, NJ were collected and characterized by XRD, XRF and wet chemical analysis. The bulky chemical composition analysis show the range for a few major metal elements: Ca (28.0-46.7%), Fe (9.2-16.0%), Al(5.6-9.5%), Mg(9.2-11.8%), Si(4.4-12.0%), Cr(2.4-3.8%). The iron content is in the low Fe range when compared with the chemistry of COPR samples from nine sites in the previous study. The XRD analysis indicates the major phase for iron is brownmillerite, and the major phase for Ca is $Ca(OH)_2$ and $CaCO_3$. The chemical composition and mineral phases will enable us to optimize metal reduction and separation by adjusting operational conditions (additive, temperature, and reaction time).

The preliminary reduction study by TGA was conducted using Sample-2S as a representative COPR sample. The reduction of iron oxide in COPR to metal was achievable under the oxygen-free environment with sufficient amount of reducing agent. The reaction occurred rapidly at high temperatures and completed during the heating period from 1000°C to 1400°C.

The metal separation was occurred when more than 20% sand was added to neutralize the large amount of CaO present in the COPR. The morphology study of the residue from TGA using SEM-EDX confirmed the reduction of iron and subsequent separation to produce a metal phase that contained mainly Fe/Cr. In the oxide phase of the TGA residue intermediate compounds, such as CaO-SiO2, were found and minimal amount of Fe/Cr were observed.

This research aims to optimize the reaction conditions, wide applicability of the process and feasibility in larger scale experiments: in high-temperature furnaces. Using a box furnace, the metal reduction and agglomeration was achievable. The mass percentage of metal recovery was 9.56, 12.74, and 12.5%, the numbers agreed well with COPR analysis. The recovery rate of Fe was as high as 82-89%, the number was a lower bound due to the potentially incomplete separation of metal from slag phase.

The metal separated had Fe/Cr ratio between 14-18%, a range of stainless steel. The metal still had high concentration of Si, which would require further refinement to bring the composition to that of stainless steel.

The removal of metal from slag phase not only provides a permanent solution to serious contamination problem it also lowers the density making it suitable for its reuse potential as construction materials.

Acknowledgements

The work described in this manuscript was supported by a research contract from the New Jersey Dept of Environmental Protection. The contents of this report reflect the views of authors. The contents do not necessarily reflect views or policies of NJIT or NJDEP. Authors would like to thank all the efforts of project manager Mr. Robert Mueller and Mr. Ravi Patraju of NJDEP.

References

Abumaizar, R. J. and Smith, E. H., (1999), "Heavy metal contaminants removal by soil washing," *Journal of Hazardous Materials*, 70(1), 71-86.

Allan, M. L. and Kukacka, L. E., (1995), "Blast furnace slag-modified grouts for in situ stabilization of chromium-contaminated soil," *Waste Management*, 15(3), 193-202.

Bafghi, M. S., M. Fukuda, Y. Ito, S. Yamada, and M. Sano, (1993) ISIJ International, Vol. 33 No.11, pp. 1125-1130.

Bogdandy, L. V. and Engell, H. J., (1971), *The Reduction of Iron Oxides*, Springer, New York.

Bonen D., and Sarkar, S. L., (1994) "The Present State-of-the-art of Immobilization of Hazardous Heavy Metals in Cement Based Materials," *Proc. of Engineering Foundation Conference on Advances in Cement and Concrete*, Durham, NH, 481-498.

Burke, T., Fagliano, J., Goldoft, M., Hazen, R. E., Tglewicz, R. and Mckee T., (1991), "Chromite Ore Processing Residue in Hudson County, New Jersey." *Environ Health. Pres*., 92, 131-137.

Burrows D, Adams R. M. (1990) *Metals In Occupational Skin Disease*, 2nd ed, WB Saunders Co, 349.

Chakraborty, Dolly; Ranganathan, S.; Sinha, S. N. Metallurgical and Materials Transactions B: Process Metallurgy and Materials Processing Science (2005), 36B(4), 437-444.

Chakraborty, Dolly; Ranganathan, S.; Sinha, S. N. Metals, Materials and Processes (2004), 16(2-3), 199-208.

Chakraborty, Dolly; Ranganathan, S.; Sinha, S. N. Transactions of the Indian Institute of Metals (2003), 56(4), 335-339.

Chakraborty, Dolly; Ranganathan, S.; Sinha, S. N. Journal of Metallurgy and Materials Science (2002), 44(1), 1-13.

Clark, R.P., et al., 1975, “Thermo-analytical Investigation of $CaCrO_4$,” *Thermochem Acta.* Vol. 33, pp.141-445.

Cronin E. (1980) *Contact Dermatitis*, Churchill Livingstone, Edinburgh, 287.

Cunningham S. D., Berti W. R., and Huang J. W., (1995) "Phytoremediation of contaminated soils," *Trends Biotechnol*, 13, 393-397.

Ding, Y. L.; Merchant, A. J. Ironmaking and Steelmaking (1999), 26(4), 247-253. Kinetics and mechanism of smelting reduction of fluxed chromite. Part 1. Carbon - chromite -flux composite pellets in Fe-Cr-C-Si melts.

Ding, Y. L.; Merchant, A. J Ironmaking and Steelmaking (1999), 26(4), 254-261. Kinetics and mechanism of smelting reduction of fluxed chromite. Part 2. Chromite-flux pellets in Fe-C-Si melts.

Ding, Y. L.; Warner, N. A (1997), Thermochimica Acta 292(1-2), 85-94

Ding, Y.L., Warner, N.A. (1997) Ironmaking and Steelmaking, 24 (4), pp. 283-287.

Ding, Y.L., Warner, N.A. (1997) Ironmaking and Steelmaking, 24 (3), pp. 224-229.

Ding, Y.L., Warner, N.A., Merchant, A.J. (1997) Scandinavian Journal of Metallurgy, 26 (2), pp. 55-63.

Duong, H. V.; Johnston, R. F Ironmaking and Steelmaking (2000), 27(3), 202-206

El-Geassy, A.A., 1996, "Gaseous Reduction of MgO-Doped Fe_2O_3 Compacts with Carbon Monoxide at 1173-1473," *ISIJ International*, Vol.36, No.11, pp.1328-1337.

El-Geassy, A.A., 1998, "Stepwise reduction of CaO and/or MgO Doped-Fe_2O_3 Compacts (Hematite-Wustite-Iron Transformation Steps)," *Scandinavian Journal of Metallurgy*, Vol. 27, pp.205-213.

Hillier, s., Roe, M. J., Geelhoed, J. S., Fraser, A. R., Farmer, J. G., and Paterson, E., (2003) "Role of quantitative mineralogical analysis in the investigation of sites contaminated by chromite ore processing residue," *The Science of the Total Environment,* 308, 195–210.

Katz, S. A., and Salem H., (1994) *Biological and Environmental Chemistry of Chromium*, VCH Publishers, NY.

Kamolpornwijit, W., (2000) "Feasibility Study to Extract Iron and Chromium from Chromium Contaminated Soils" Dissertation submitted to the New Jersey Institute of Technology in partial fulfillment of the requirement for the degree of Doctor of Philosophy.

Lekatou, A., Walker, R.D.(1995) Ironmaking and Steelmaking, 22 (5), pp. 378-392.

Lekatou, A., Walker, R.D. (1995) Ironmaking and Steelmaking, 22 (5), pp. 393-404.

Lekatou, A., and R.D. Walker, 1997, "Effect of SiO_2 Addition on Solid State Reduction of Chromite Concentrate," *Ironmaking and Steelmaking*, Vol.24, No.2, pp.133-143.

Lourenco, J. C. N. and Alvim-Ferraz, M. C. M., (1999), "Extraction of chromium from contaminated soils," International Journal of Environmental Analytical Chemistry, *The 2nd Euro-conference on Environmental Analytical Chemistry*, 33-42.

Meegoda, J. N., Librizzi, B., McKenna, G. F., Kampolpornwijit, W., Cohen, D., Vaccari, D. A., Ezeldin, A. S., Walden, L., Noval, B. A., Mueller, R. T. and Santora S., (1995), "Remediation and Reuse of Chromium Contaminated Soils Through Cold Top In-situ Vitrification," *Proc. of the 27th. Mid-Atlantic Industrial Waste Conference*, Bethlehem, PA, July 9-12, 733-742.

Meegoda, J. N., Kamolpornwijit, W., Vaccari, D. A., Ezeldin, A. S., Noval, B. A., Mueller, R. T. and Santora, S., (1999), "Remediation of Chromium Contaminated Soils - A Bench-scale Investigation," *ASCE Practice Periodical of Hazardous, Toxic, and Radioactive Waste Manag.t*, 3(3), 124-131.

Meegoda, J. N., Partymiller, K., Richards, M. K., Kamolpornwijit, W., Librizzi, W., Tate, T., Noval, B. A., Mueller, R. T. and Santora, S., (2000), "Remediation of Chromium Contaminated Soils -A Pilot Scale Investigation," *ASCE Practice Periodical of Hazardous, Toxic, and Radioactive Waste Management*, 4(1), 7-15.

Mroz, J., (1994) Scandinavian Journal of Metallurgy, Vol. 23, pp. 171-183.

Muan, A., Osborn, E. F., 1965, Phase Equilibria among Oxides in Steelmaking, Addison Wesley, Reading Massachusetts.

Nafziger, Ralph H., Tress, Jack E., Paige, Jack I. (1979) Metall Trans B, 10 B (1), pp. 5-14.

Nasr, M. I., A.A. Omar, M.H. Khadr, and A.A. El-Geassy, 1994, “Analysis of Solid-State Reduction of Iron Ore from a Couple of Experimental Measurements,” *Scandinavian Journal of Metallurgy*, Vol. 23, pp.119-125.

Pagilla, K. R. and Canter, L. W., (1999), "Laboratory Studies on Remediation of Chromium-Contaminated Soils," *Journal of Environmental Engineering*, 125(3), 243-248.

Perry, K.P.D., Finn, C.W.P., King, R.P. (1988) Metallurgical transactions. B, Process metallurgy, 19 (4), pp. 677-684.

Probstein, R. F. and Gehring, G. A., (1997) *In-Situ Field Test of Electroremediation of a Chromate-Contaminated Site in Hudson County, New Jersey*, Final report to Northeast Hazardous Substance Research Center, Newark, NJ.

Srinivasan, N.S., and A.K. Lahiri, 1977, “Studies on the Reduction of Hematite by Carbon,” Metal. Trans. B., Vol.8B, pp.175.

Sugata, M., T. Sugiyama and S. Kondo, 1974, “Reduction of Iron Oxide Contained in Molten Slags with Solid Carbon,” Trans. Iron Steel Inst Jpn. Vol.14. pp.88-95.

Sundar Murti, N.S., Seshadri, V. (1982) Transactions of the Iron and Steel Institute of Japan, 22 (12), pp. 925-933.

Sundar Murti, N.S., Seshadri, V. (1985) Transactions of the Indian Institute of Metals, 38 (5), pp. 423-425.

Szendrei, T.; Van Berge, P., 1988, Thermochim. Acta, 44 , 11Sturges, S. G., McBeth, P. C. and Pratt, R. C., (1991), "Performance of soil flushing and groundwater extraction at the United Chrome Superfund site," *Journal of Hazardous Materials*, 29(1), 59-78.

Taggart, A. F, (1947) *Handbook of Mineral Dressing, Ores and Industrial Minerals*, Wiley, NY.

Tai, H. and Jou, C. G., (1999), "Immobilization of chromium-contaminated soil by means of microwave energy," *Journal of Hazardous Materials*, 65(3), 267-275.

Udy, M.J., (1956), *Chromium Vol.1, Reinhold, NY.*

Van Deventer, J. S. J. (1988) Thermochimica Acta 127, 25-35.

Van Vuuren, C. P. J.; Bodenstein, J. J.; Sciarone, M.; Kestens, P. Symposium Series - South African Institute of Mining and Metallurgy, vol S11, issue INFACON 6, Vol. 1, 51-55

Vazarlis, H.G., Lekatou, A. (1993) Ironmaking and Steelmaking, 20 (1), pp. 42-53.

Wang, S. and Vipulanandan, C., (2001), "Solidification/stabilization of Fe(II)-treated Cr(VI)-contaminated soil," *Environmental Engineering Science*, 18(5), 301-308.

Weber, P.; Eric, R. H. (1993), Metallurgical Transactions B: Process Metallurgy 24B(6), 987-95.

USEPA (1989), US Environmental Protection Agency, “Stabilization/Solidification of CERCLA and RCRA Wastes, Physical Tests, Chemical Testing Procedures, Technology Screening, and Field Activities,” EPA/625/6-89/022, May.

USEPA (1992) “Vitrification Technologies for Treatment of Hazardous and Radioactive Waste.” Office of Research and Development Washington DC. EPA/625/R-92/002, May 1992 USEPA (1983), US Environmental Protection Agency, "Methods for Chemical Analysis of Water and Waste," Environmental Monitoring and Support Laboratory, Cincinnati, Ohio, EPA-600/4-79-020.

USEPA (1994), US Environmental Protection Agency, "Test Methods for Evaluating Solid Waste," Physical/Chemical Methods, Laboratory Manual, Volumes IA through IC and Field Manual, Volume 2. SW-846, Third Edition (Revision II and IIA), Office of Solid Waste and Emergency Response, September.

USEPA (1996), US Environmental Protection Agency, "Draft Quality Assurance Project Plan for the Geotech Development Corporation Cold Top *Ex*-Situ Vitrification System Technology Demonstration in Niagara Falls, New York; New Jersey Chromium Sites," National Risk Management Research Laboratory, November.

USEPA, (1998), US Environmental Protection Agency, "Geotech Development Corporation Cold Top Ex-Situ Vitrification Technology SITE Program Demonstration Innovative Technology Evaluation Report," Office of Research and Development, Cincinnati, Ohio, August.